Electro-coflow Simulation Using Dual Grid Level Set Method

Author:
Rohit Nikam

Supervisor:
Prof. Venkat Gundabala

A thesis submitted in fulfilment of the requirements for the degree of

Master of Technology

Department of Chemical Engineering
Indian Institute of Technology Bombay
India

June, 2015

Declaration of Authorship

I, Rohit Nikam, declare that this thesis titled, 'Electro-coflow Simulation Using Dual Grid Level Set Method' and the work presented in it are my own. I confirm that:

- This work was done wholly or mainly while in candidature for a research degree at this University.
- Where any part of this thesis has previously been submitted for a degree or any other qualification at this University or any other institution, this has been clearly stated.
- Where I have consulted the published work of others, this is always clearly attributed.
- Where I have quoted from the work of others, the source is always given. With the exception of such quotations, this thesis is entirely my own work.
- I have acknowledged all main sources of help.
- Where the thesis is based on work done by myself jointly with others, I have made clear exactly what was done by others and what I have contributed myself.

Signed: _____

Date: _____

INDIAN INSTITUTE OF TECHNOLOGY BOMBAY

Abstract

Department of Chemical Engineering

Master of Technology

Electro-coflow Simulation Using Dual Grid Level Set Method

by Rohit NIKAM

The present work aims to contribute for the study of electrohydrodynamics of the system of coflowing liquids via simulation and analysis. A mathematical formulation introducing the field of electrohydrodynamics is presented at first, including Maxwell's equations, constitutive laws and conservation equations. Governing equations for an axisymmetric case of charge transport in a cone-jet mode through leaky dielectric fluid co-flowing with another dielectric fluid are framed and using them 2D transient Computational Multi-Fluid Dynamics simulation of the system is performed with the help of Dual Grid Level Set Method. Results are analysed for three independently varying system parameters – electric potential, ratio of inlet average velocities of fluids and viscosity ratio of fluids. It has been found that within a given parametric domain, electrohydrodynamic jet stability increases with increasing the electric potential and the viscosity ratio and the inner fluid changes from jet to microdripping flow mode on increasing the inlet average velocity ratio.

Acknowledgements

I sincerely thank Prof. Venkat Gundabala for his kind support and a number of fruitful discussions. I am also grateful to Prof. Atul Sharma for providing me with the code and a high performance computational facility for this study. I am especially thankful to the members of CFDHT lab, Department of Mechanical Engineering, IITB. I am thankful to Prof. Absar Lakdawala for clearing my doubts in the topic and to Mr. Javed Shaikh for always assisting and directing me with the theoretical and computational aspects of the work.

I acknowledge the constant support by my family. I thank my mother and father for always being there for me during every stage.

Rohit Nikam
IIT Bombay

June, 2015

Contents

Declaration of Authorship i

Abstract ii

Acknowledgements iii

Contents iv

List of Figures vi

Symbols vii

1 Introduction 1
- 1.1 Overview . . . 1
- 1.2 Literature Review . . . 2

2 Basics of Electrohydrodynamics : Mathematical Formulation 4
- 2.1 Conservation of Mass . . . 5
- 2.2 Balancing Linear Momentum . . . 6
- 2.3 Conservation of Charge . . . 8
- 2.4 Maxwell's Equations . . . 9
- 2.5 Scaling Analysis: Non-dimensional Maxwell's Equations . . . 11
- 2.6 Electroquasistatics . . . 12
- 2.7 Electrical Forces . . . 13
- 2.8 Boundary Conditions at the Interface . . . 14
  - 2.8.1 Electric Field and Potential at the Interface . . . 14
  - 2.8.2 Velocities at the Interface . . . 16
  - 2.8.3 Equilibrium of Forces at the Interface . . . 17
    - 2.8.3.1 Tangential Stress Balance . . . 19
    - 2.8.3.2 Normal Stress Balance . . . 19

3 Electro-coflow Simulation 20
- 3.1 Modelling Interface Dynamics - A Level Set Approach . . . 21
  - 3.1.1 Functions used in the level set method . . . 23
    - 3.1.1.1 Level Set Function . . . 23
    - 3.1.1.2 Heaviside Function . . . 24
    - 3.1.1.3 Dirac Delta Function . . . 27

3.1.2 Governing equations for the level set function 28
3.1.2.1 Volume Conservation Equation 29
3.1.2.2 Mass Conservation (Level Set Advection Equation) . . . 31
3.1.2.3 Subsidiary Equation: Re-initialization 32
3.1.2.4 Momentum Equations 33
3.1.2.5 Governing Equations for Electric Field 35
3.1.3 Numerical Methodology 37
3.1.3.1 Dual grid Arrangement 37
3.1.3.2 Numerical Solution of Navier-Stokes and Level Set Equations 38
3.1.3.3 Electric Field: Solution of Laplace Equation for Electric Potential 38
3.1.3.4 Calculation of Source Term for Electric Body Force . . . 38
3.1.3.5 Solution Algorithm 41
3.2 Results and Discussion 42
3.2.1 Parametric Details 42
3.2.2 Interface dynamics of Electrified Jet 43
3.2.3 Effect of Change in the Ratio of Average Inlet Velocities 43
3.2.4 Effect of Change in Electric Potential 48
3.2.5 Effect of Change in the Viscosity Ratio 51
3.3 Conclusion 53

List of Figures

2.1 Control volume for charge conservation 9
2.2 Interface between two fluids 14
2.3 Line integral across the interface 15
2.4 Coordinate system for locating the interface 16

3.1 System of interest 20
3.2 Contours of level set function 23
3.3 Interface representation according to level set method 23
3.4 Smoothed Heaviside function 26
3.5 Interface thickness in level set method 26
3.6 Control volume in level set method 27
3.7 Smoothed Dirac Delta function 28
3.8 Control volume representation for volume conservation equation 29
3.9 Control volume representation for mass conservation equation 29
3.10 A representative 2-D axisymmetric electro-multifluid-dynamics system . . 31
3.11 Staggered grid points for traditional level set method 39
3.12 Staggered control volumes for traditional level set method 39
3.13 Staggered grid points for dual grid level set method 40
3.14 Staggered control volumes for dual grid level set method 40
3.15 Discretization of electric field equations 41
3.16 EHD jet evolution with varying ratio of average inlet velocities 45
3.17 EHD jet length for different ratios of average inlet velocities 47
3.18 EHD jet evolution for different electric Bond numbers 50
3.19 EHD jet length for different electric Bond numbers 52
3.20 EHD jet evolution for different viscosity ratios 54

Symbols

$\mathbf{D}$	Non-dimensional electric displacement vector
$\mathbf{E}$	Non-dimensional electric field vector
$\mathbf{J}$	Non-dimensional current density vector
q_v	Volumetric charge density
R_1	Non-dimensional drop/jet radius
R_2	Non-dimensional domain length in radial direction
U	Non-dimensional velocity component in radial direction
V	Non-dimensional velocity component in axial direction
Z	Non-dimensional length in axial direction
R	Non-dimensional length in radial direction
α	Electric permittivity ratio
β	Electric conductivity ratio
γ	Interfacial tension
δ	Dirac delta function
ϵ	Diffused interface thickness
η	Viscosity ratio
κ	Interface curvature
ρ	Mass density of the medium
K	Electrical conductivity of the medium
ϕ	Level set function
χ	Mass density ratio
Θ	Non-dimensional electric potential

Dedicated to my parents - Sunanda and Manikrao Nikam

Chapter 1

Introduction

1.1 Overview

Electrohydrodynamics is the study of fluid dynamics under electric field. If an electrically conducting fluid is subjected to an electric field, the charge inside the fluid comes on the surface and an electric stress gets applied on the surface of the fluid. In case of homogeneously dielectric fluid, molecules of the fluid get polarized and net charge due to such polarization appears at the surface. The charge accumulated at the interface due to migration from the bulk is called free charge while the charge which appears due to polarization is called bound charge. The presence of an electric field creates force on these charges and the fluid "feels" a force at its interface. Such interfacial force is normal to the interface in case there are no free charges or electrons in the bulk of a fluid i.e. the fluid is perfectly dielectric while this force also has a tangential component in case the fluid is conducting or leaky dielectric. Various time scales arise in the overall dynamics of fluid under the action of electric field. The charge relaxation time scale is the average time taken by charges inside the conductor to come to the surface from bulk. Convection time scale is the average time taken by fluid element to cover certain characteristic length. Viscous relaxation time is the characteristic time taken for the decay of viscous stresses. During transient motion of fluid when viscous forces are comparable to electric forces, electroviscous time scale plays substantial role. Similarly electro-inertial time scale becomes significant when inertial forces are of the same magnitude as electric forces.

The stability of an interface is notably influenced by the presence of an electric field. Electric field has been understood as an effective tool for acting as a gravitational force, for separating or mixing of two fluids, breakup of liquid droplets and bubbles, generating

droplets from a liquid jet on demand, etc. So detailed understanding of the multi-phase fluid dynamics under the influence of external electric field is essential in order to efficiently control such processes.

1.2 Literature Review

When an electric field is applied on a fluid meniscus, meniscus gets stretched in the direction of electric field. This results in a deformation of meniscus and is proportional to the intensity of electric field applied and the curvature of surface starts increasing at one point with increasing electric field. At some threshold of electric field, a liquid jet gets emitted from that point. If we have continuously flowing liquid with sufficient intensity of electric field, the liquid meniscus at the exit forms a shape of a cone with an apex from which a continuous jet emanates and eventually forms into droplets. The jet carries an electric current which is composed of convection current due to interfacial charges and bulk conduction current. The cone formed is known as the Taylor cone. If the intensity of electric field is increased more, unusual behaviour of jet whipping is seen. Previous works by Zeleny [1–3], Taylor [4] have explained the reason for the existence of Taylor cone to be hydrostatic equilibrium between electric stress and stress due to interfacial tension. The dynamics of drop formation in dripping regimes was studied experimentally by Takamatsu [5, 6], Zhang and Basaran [7]. Cloupeau and Prunet-Foch [8] experimentally determined the domain of operation or region of the voltage/ flow rate plane where a cone-jet of a given liquid can be established. This region is bounded by a minimum voltage that depends on the flow rate and at which the system jumps to an oscillatory mode, and a maximum voltage above which instabilities, or a multiple-jet mode, or electrical discharges in the surrounding gas appear. The flow rate can be varied at constant voltage in the domain of operation between certain minimum and maximum values. Cloupeau and Prunet-Foch [8] have experimentally found that there exists a minimum flow rate of the liquid in order to see the cone-jet regime. The jet part has convection current dominating conduction current while conduction current has major contribution in the meniscus part. Fernandez de la Mora and Loscertales [9] investigated a geometrical regime where there is equal contribution from both currents and have found that if the liquid has considerably high electric conductivity and the liquid flow rate is not very large than minimum required for con-jet regime, the electric current only depends on the flow rate and the physical properties of liquid, in fact the current varies as square root of the flow rate. The breakup of the jet into drops is most regular near this minimum flow rate, leading to the smallest drops and the narrowest size distributions (Rosell Llompart and Fernandez De La Mora [10]).
The jet formed is considerably thin and the size of droplets in which the jet breaks is from

tens of nanometers to tens of micrometers. This aspect is exploited for the formation of monodisperse drops and fibers via electrospinning and electrospraying. Gundabala, Vilanova and Fernandez-Nieves [11] did an electrospraying in microfluidic device in which a co-flow of dielectric oil surrounded the flow of conducting, viscous liquid and have found that the current increases linearly with applied voltage and is weakly dependent on the flow rate of the liquid. It was shown experimentally that the current in this case is a surface convection current due to electric stresses at the surface and not the conduction current.

Recently, numerical simulations is used to investigate the formation mechanism of the Taylor cone and jet. Gañán-Calvo [12], Hartman [13, 14], Higuera [15] have presented one dimensional models for simulation of electrified jet in cone jet mode. Using Finite Element based one dimensional model, Nots and Basaran [16] have proposed gross dynamics in dripping and microdripping regimes. Unfortunately, such 1D simulations are unable to capture breakup of the jet as well as any radial motion of the fluid inside the jet. The recent development of interface tracking method for multiphase flow simulation has provided a novel and robust numerical approach to treat the moving interface between two immiscible fluids. Lim [17] and Herrada [18] used front tracking and volume of fluid method respectively to simulate cone jet formation.

Chapter 2 of the thesis consists of the basic theoretical foundation behind electrohydrodynamic phenomena. The analysis of the present case of electro-coflow starts from chapter 3 with a system description. It is followed by an introduction of an analytical framework for solving this system- a level set approach which formulates the governing equations for interface dynamics. Based on this, a novel numerical algorithm developed by Gada and Sharma [19] called dual grid level set method is presented and implemented. The last section presents the results and their interpretations with final conclusions.

Chapter 2

Basics of Electrohydrodynamics : Mathematical Formulation

A fluid can be modelled as a continuum in which velocity, density are continuous functions of position.
Eulerian and Lagrangian description are the two ways to specify a position of a given element of a fluid. In the Eulerian framework, we describe the flow quantities as a function of independent variables position and time, while in the Lagrangian framework, the position at a particular time is specified as a function of its initial position.
A quantity $f(x,t)$ for a fixed fluid particle in a velocity field $\mathbf{u}(x,t)$ varies in time according to its substantial derivative or material derivative which is given by

$$\frac{df}{dt} = \frac{f\left(x+dx, t+dt\right) - f\left(x,t\right)}{dt} = \frac{\partial f}{\partial t} + \mathbf{u}\cdot\nabla f$$

where one fact which is used is that the displacement of a particle in a time interval dt is given by $dx(x,t) = \mathbf{u}(x,t)dt$. For example, the acceleration of a fluid particle is given by

$$a = \frac{d\mathbf{u}}{dt} = \frac{\partial \mathbf{u}}{\partial t} + \mathbf{u}\cdot\nabla\mathbf{u}$$

$\nabla\rho$ and $\nabla\mathbf{u}$ contain the information of the local variations of the mass density and the velocity field. $\nabla\mathbf{u}$ is a tensor which is decomposed into symmetric and antisymmetric parts as

$$\nabla\mathbf{u} = \frac{1}{2}\left(\nabla\mathbf{u} + \nabla\mathbf{u}^T\right) + \frac{1}{2}\left(\nabla\mathbf{u} - \nabla\mathbf{u}^T\right) = \mathbf{e}_i e_{ij}\mathbf{e}_i + \mathbf{e}_i w_{ij}\mathbf{e}_i$$

where, $\mathbf{u}^T$ is is a transpose tensor and $\mathbf{e}_i$, $i = 1,2,3$ are the unit vectors of the Cartesian system of coordinates and

$$e_{ij} = \frac{1}{2}\left(\frac{\partial u_i}{\partial x_j} + \frac{\partial u_j}{\partial x_i}\right)$$

$$w_{ij} = \frac{1}{2}\left(\frac{\partial u_i}{\partial x_j} - \frac{\partial u_j}{\partial x_i}\right)$$

To see the significance of this, let us assume a fluid particle as an origin of a frame of reference which is moving along with it. The distance of the fluid particle adjacent to it was $\Delta l(0)$ at time $t = 0$. At time Δt, the distance becomes

$$\Delta l(\Delta t) = \Delta l(0) + (\nabla \mathbf{u} \cdot \Delta l)\Delta t$$

In the limit of $\Delta t \to 0$, replacing all incremental quantities by differentials, defining the unit vector $\mathbf{n} = \mathbf{dl}/dl$, using above equation, the rate of dilatation of $\mathbf{dl}$ is given by

$$\frac{\mathbf{n} \cdot \nabla \mathbf{u} \cdot \mathbf{n} dl dt}{dt} = (\mathbf{n} \cdot \mathbf{e} \cdot \mathbf{n} + \mathbf{n} \cdot \mathbf{w} \cdot \mathbf{n})\, dl = \mathbf{n} \cdot \mathbf{e} \cdot \mathbf{n} dl$$

Since, $\mathbf{n} \cdot \mathbf{w} \cdot \mathbf{n} = \mathbf{e}_i n_i n_j w_{ij} \mathbf{e}_j = 0$ because $\mathbf{n}_i \mathbf{n}_j$ is a symmetric tensor and $\mathbf{w}_{ij}$ is an antisymmetric tensor. Extending this to three dimensions by taking $\mathbf{dl} = dx_i \mathbf{e}_i$, the rate of dilatation of volume dV is given by

$$\frac{dV\,(dt) - dV\,(0)}{dt} = (e_{11} + e_{22} + e_{33})\, dV\,(0) = (Tr\,(\mathbf{e}))\, dV = (\nabla \cdot \mathbf{u})\, dV$$

We see that the tensor $e = \mathbf{e}_i e_{ij} \mathbf{e}_j$ gives the rate of deformation or dilatation of a fluid element. Analogous procedure can be performed to show that $w = \mathbf{e}_i w_{ij} \mathbf{e}_j$ gives the rotation of a rigid body element. One of the key assumptions for the analysis is that the fluid flow is irrotational which sets $\mathbf{w} = 0$.

2.1 Conservation of Mass

Consider an arbitrary shaped fluid element through which the fluid is flowing. Performing the mass balance across the volume gives

$$\int_V \frac{\partial \lambda}{\partial t} dV + \int_S \lambda \mathbf{u} \cdot \mathbf{n} dS = 0$$

where λ is the fluid mass density. V is the volume of the fluid element. S is the surface area closed figure having a unit normal $\mathbf{n}$ at any point. The first term on the left hand side is the rate of accumulation of fluid mass inside the volume and second term is the difference between net mass flux outside and net mass flux inside of the volume. The source/sink term on the right hand side should be zero since mass cannot be created or depleted.

Using the divergence theorem on the second term on the left hand side, we get

$$\int_V \frac{\partial \lambda}{\partial t} dV + \int_V \nabla \cdot (\lambda \mathbf{u})\, dV = 0$$

$$\frac{\partial \lambda}{\partial t} + \nabla \cdot (\lambda \mathbf{u}) = 0$$

Note that since no assumption is considered so far, this equation is universal and is also called *the continuity equation.*
Expanding the divergence term,

$$\frac{\partial \lambda}{\partial t} + \lambda \nabla \cdot \mathbf{u} + (\mathbf{u} \cdot \nabla)\, \lambda = 0$$

Now we assume that the mass density of the fluid remains constant spacially and temporally throughout the system, this results in

$$\nabla \cdot \mathbf{u} = 0$$

This is the condition for the incompressibility of a fluid, which implies that the volume of the fluid element remains constant. Hence both the dilatational and the rotational parts of the gradient of the velocity field are zero in our case.

2.2 Balancing Linear Momentum

Newton's second law should be applied to the fluid element to conserve its momentum. Considering the fluid element discussed above, its net rate of change of momentum should be equal to the difference in the convective flux through the surface enclosing the fluid element, plus the rate of change of momentum due to body forces and surface forces on the element.

$$\int_V \frac{\partial \lambda \mathbf{u}}{\partial t} dV + \int_S \lambda \mathbf{u}\mathbf{u} \cdot \mathbf{n} dS = \int_V \mathbf{f}_B dV + \int_S \mathbf{f}_S dS$$

where $\mathbf{f}_B$ is the body force per unit volume and $\mathbf{f}_S$ is the surface force per unit area of fluid element. Let us call $\mathbf{f}_S$ as $\mathbf{f}$ for further discussions.
Surface force can be divided into forces normal and tangential to the surface S enclosing the fluid element. The infinitesimal force $\delta\mathbf{f}$ acting on the element $\delta\mathbf{S} = \mathbf{n}\delta S$ is usually decomposed like

$$\delta\mathbf{f} = -p\mathbf{n}\delta S + \sigma_n \delta S \tag{2.1}$$

where p is the thermodynamic pressure which is independent of the direction of the unit normal $\mathbf{n}$ to the surface S whereas, the quantity σ_n here depends on the normal to the surface. σ is the viscous stress tensor and its component normal to the surface is given by σ_n. Viscous stress tensor σ is given by

$$\sigma = \begin{bmatrix} \sigma_{xx} & \sigma_{xy} & \sigma_{xz} \\ \sigma_{yx} & \sigma_{yy} & \sigma_{yz} \\ \sigma_{zx} & \sigma_{zy} & \sigma_{zz} \end{bmatrix}$$

The normal component of viscous stress tensor, σ_n is given by

$$\sigma_n = \sigma_{e_i}\mathbf{n}\cdot\mathbf{e}_i = \mathbf{n}\cdot\mathbf{e}_i\sigma_{ij}\mathbf{e}_j$$

From the conservation of angular momentum, we get

$$\sigma_{ij} = \sigma_{ji}$$

which means that the viscous stress tensor is symmetric. Hence we characterize the state of stresses at each point by the mechanical stress tensor $\mathbf{T}$ such that

$$T_{ij} = -p\delta_{ij} + \sigma_{ij}$$

or

$$\mathbf{T} = -p\mathbf{I} + \sigma \tag{2.2}$$

where $\mathbf{I}$ is the identity matrix. So we can write equation (2.1) as

$$\delta\mathbf{f} = \mathbf{T}\cdot\mathbf{n}\delta S$$

Modifying the overall momentum conservation equation

$$\int_V \frac{\partial\lambda\mathbf{u}}{\partial t}dV + \int_S \lambda\mathbf{u}\mathbf{u}\cdot\mathbf{n}dS = \int_V \mathbf{f}_B dV + \int_S \mathbf{T}\cdot\mathbf{n}dS$$

Using the divergence theorem for the second term on the right hand side and second term on the left hand side gives

$$\int_V \frac{\partial\lambda\mathbf{u}}{\partial t}dV + \int_V \nabla\cdot(\lambda\mathbf{u}\mathbf{u})\,dV = \int_V \mathbf{f}_B dV + \int_V \nabla\cdot\mathbf{T}dV$$

$$\frac{\partial\lambda\mathbf{u}}{\partial t} + \nabla\cdot(\lambda\mathbf{u}\mathbf{u}) = \mathbf{f}_B + \nabla\cdot\mathbf{T}$$

Rewriting the left hand side

$$\frac{\partial \lambda \mathbf{u}}{\partial t} = \lambda \frac{\partial \mathbf{u}}{\partial t} + \mathbf{u} \frac{\partial \lambda}{\partial t}$$

and

$$\nabla \cdot (\lambda \mathbf{u}\mathbf{u}) = \mathbf{u} \nabla \cdot (\lambda \mathbf{u}) + \lambda \left(\mathbf{u} \cdot \nabla\right) \mathbf{u}$$

So

$$\frac{\partial \lambda \mathbf{u}}{\partial t} + \nabla \cdot (\lambda \mathbf{u}\mathbf{u}) = \lambda \left[\frac{\partial \mathbf{u}}{\partial t} + \left(\mathbf{u} \cdot \nabla\right) \mathbf{u} \right] = \lambda \frac{d\mathbf{u}}{dt}$$

Note that the term on the right hand side is the substantial derivative of the fluid velocity. Hence the momentum conservation equation becomes

$$\lambda \frac{d\mathbf{u}}{dt} = \mathbf{f}_B + \nabla \cdot \mathbf{T} \tag{2.3}$$

Most of the fluids are characterized by the constitutive relation

$$\sigma = 2\mu \left(\mathbf{e} - \frac{1}{3} e_{ii} \mathbf{I} \right) + \eta e_{ii} \mathbf{I} \tag{2.4}$$

where $\mathbf{e}$ is the rate of deformation tensor and μ and η are the first and second coefficients of viscosity.

$$Tr\left(\mathbf{e}\right) = e_{ii} = \nabla \cdot \mathbf{u} \tag{2.5}$$

Combining equations (2.2), (2.3), (2.4) and (2.5), we get

$$\lambda \frac{d\mathbf{u}}{dt} = -\nabla p + \mu \nabla^2 \mathbf{u} + \left(\eta + \frac{1}{3} \mu \right) \nabla \left(\nabla \cdot \mathbf{u} \right) + \mathbf{f}_B$$

This is called the famous *Navier-Stokes equation*. If the fluid is assumed incompressible, this equation reduces to

$$\lambda \frac{d\mathbf{u}}{dt} = -\nabla p + \mu \nabla^2 \mathbf{u} + \mathbf{f}_B$$

The electrical forces on the fluid element will be included in the body force term in the RHS of the equation.

2.3 Conservation of Charge

Just like the simple mass balance, the equation for charge balance can be generated. In a continuum approximation, let us consider the volume element with volume V, surface area S, the normal to the surface at any point as $\mathbf{n}$, the charge density of a fluid as ρ which can vary spacially or temporally, the source (or sink) of charge generation (or depletion) inside the volume be $\mathbf{P}$, the velocity of a fluid flowing as $\mathbf{u}$. See figure 2.1. Applying the charge balance gives

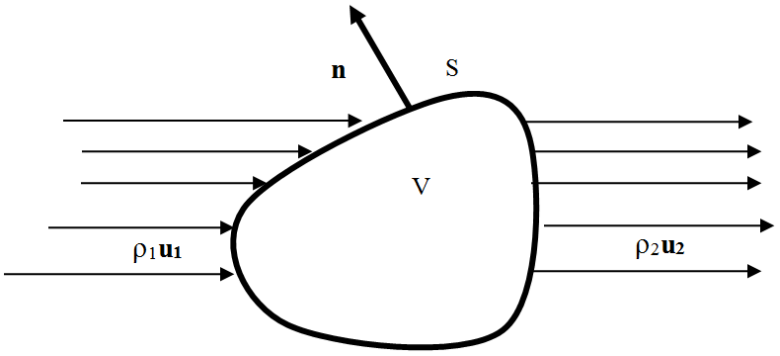

FIGURE 2.1: Control volume for charge conservation

$$\int_V \frac{\partial \rho}{\partial t} dV + \int_S \rho \mathbf{u} \cdot \mathbf{n} dS = \int_V \mathbf{P} dV$$

where first term on the left hand side is the charge accumulation term, second term is the difference between the net incoming and net outgoing charge flux. The term on the right hand side is the net rate of generation (or depletion) of charge inside the volume V.

Using the divergence theorem for the second term on the left hand side,

$$\int_V \frac{\partial \rho}{\partial t} dV + \int_S \nabla \cdot (\rho \mathbf{u})\, dV = \int_V \mathbf{P} dV$$

$$\frac{\partial \rho}{\partial t} + \nabla \cdot (\rho \mathbf{u}) = \mathbf{P}$$

We know that the net charge cannot be created or depleted, which sets $\mathbf{P} = 0$

$$\frac{\partial \rho}{\partial t} + \nabla \cdot \mathbf{J} = 0$$

where $\mathbf{J}$ is the flux of electric current or the bulk current density.

2.4 Maxwell's Equations

This set of equations governs the behaviour of electric and magnetic fields, how they can distribute themselves or what configuration they can take. These equations describe what kind of physical phenomena can give rise to electric and magnetic fields.

First equation is the Gauss' law which is given by

$$\epsilon \nabla \cdot \mathbf{E} = \rho_f + \rho_b$$

where ρ_f and ρ_b are the ensemble averaged charge densities due to free charges and bound charges in the volume respectively. ϵ is the electric permittivity of the medium. $\mathbf{E}$ is the electric field in the volume. For any material inside volume V, since the net bound charge is always zero,

$$\int_V \rho_b dV = 0$$

Polarization vector or the polarization charge density $\mathbf{P}$ corresponds to the realignment of bound charges in the medium and is related to the bound charge density as

$$\rho_b = -\nabla \cdot \mathbf{P} \tag{2.6}$$

So, Gauss' law can now be written as

$$\nabla \cdot \mathbf{D} = \rho_f$$

where $\mathbf{D}$ is the electric displacement vector and

$$\mathbf{D} = \epsilon_0 \mathbf{E} + \mathbf{P}$$

Unlike the electric field, there are no scalar sources for the magnetic field, which is denoted by second Maxwell's equation as

$$\nabla \cdot \mathbf{B} = 0$$

According to Faraday's law, time varying magnetic field gives rise to the electric field as

$$\nabla \times \mathbf{E} = -\frac{\partial \mathbf{B}}{\partial t}$$

Fourth equation is the modified Ampere's law which signifies that the current density due to both free and bound charges and the magnetic field induced by the time varying electric field are the vector sources of the magnetic field.

$$\frac{1}{\mu_0} \nabla \times \mathbf{B} = \mathbf{u}_f \rho_f + \mathbf{u}_b \rho_b + \epsilon_0 \frac{\partial \mathbf{E}}{\partial t}$$

where $\mathbf{u}_f$ and $\mathbf{u}_b$ are the velocities of free and bound charges respectively and μ_0 is the magnetic permeability of vacuum.
The charge conservation for bound charges can be written as

$$\frac{\partial \rho_b}{\partial t} + \nabla . (\mathbf{u}_b \rho_b) = 0 \tag{2.7}$$

Using equations (2.6) and (2.7), we can write

$$\mathbf{u}_b \rho_b = \frac{\partial \mathbf{P}}{\partial t}$$

So the equation for fourth law can be re-written as

$$\frac{1}{\mu_0} \nabla \times \mathbf{B} = \mathbf{u}_f \rho_f + \frac{\partial \mathbf{D}}{\partial t}$$

where, $\mathbf{J} = \mathbf{u}_f \rho_f = K\mathbf{E}$ is the Ohmic conduction current density. K is the electric conductivity of the medium. So the final form is

$$\frac{1}{\mu_0} \nabla \times \mathbf{B} = \mathbf{J} + \frac{\partial \mathbf{D}}{\partial t}$$

2.5 Scaling Analysis: Non-dimensional Maxwell's Equations

Deciding the spacial and temporal scales of the overall dynamics of the system is crucial in observing the relative magnitude of the driving forces for the dynamics. In general, we have multiple characteristic time scales corresponding to various processes going on in the system.

Consider a physical system with characteristic length scale l and characteristic time scale τ. Assuming negligible polarization in the medium and for the reasons of simplicity, we assume the constitutive relations $\mathbf{D} = \epsilon\mathbf{E}$, $\mathbf{J} = K\mathbf{E}$ are valid, where ϵ and K are electric permittivity and electric conductivity of the medium and are assumed to be constants. We will use the characteristic length and time scale which we have defined above, to nondimensionalize the coordinates and time. Here we are assuming the non-relativistic motion of fluids i.e. the velocity scale of fluids is very small as compared to that of electromagnetic radiation ($u << c$). So, apparently the time scale associated with electromagnetic phenomena is very small as compared to the system time scale ($\tau >> l/c$).

Another assumption which we are considering is the negligible magnitude of magnetic field compared to that of electric field. This case is denoted as *electroquasistatics*. The case where the magnitude of electric field is assumed to be negligible as compared to that of magnetic field is called *magnetoquasistatics*. Magnetic field unlike electric field, is not being imposed externally on the system. It may be induced only due to transient charge transport in the system which can create a nonzero time derivative of electric field. Again, this depends on the time scale which we are choosing. If the chosen time

scale falls in the transient region, we can have a magnetic field along with time varying electric field.

2.6 Electroquasistatics

In this case, we assume the energy due to electric field to be very large in magnitude compared to the energy due to the induced magnetic field.

$$\frac{\epsilon E^2/2}{B^2/2\mu} = \frac{E^2}{c^2 B^2} > 1$$

Now we choose electric field to nondimensionalize Maxwell's equations. Let us assume the characteristic electric field to be E_0 in magnitude. We assume that l is the also the length scale over which the electric field varies on the order of itself. Using Gauss' law, the scale for the charge density comes out to be

$$\rho = \epsilon \frac{E_0}{l}$$

Considering the fourth Maxwell's equation

$$\frac{1}{\mu_0} \nabla \times \mathbf{B} = K\mathbf{E} + \epsilon_0 \frac{\partial \mathbf{E}}{\partial t}$$

Taking the ratio of terms on the right hand side,

$$\frac{\epsilon(\partial E/\partial t)}{KE} \sim \frac{(\epsilon/\sigma)}{\tau} = \frac{\tau_e}{\tau} \tag{2.8}$$

where the new time scale $\tau_e = \epsilon/K$, is the characteristic time for the relaxation of charge due to Ohmic conduction. The charge conservation equation can now be modified as

$$\frac{\partial \rho}{\partial t} + \nabla \cdot (K\mathbf{E}) = 0$$

Using Gauss' law

$$\frac{\partial \rho}{\partial t} + \frac{K}{\epsilon}\rho = 0$$

Integration gives

$$\rho\,(t) = \rho\,(0)\, e^{-t/\tau_e}$$

This shows that the charge in the bulk decays exponentially to zero and appears on the surface with the characteristic time τ_e. Observing equation (2.8), we see that depending on the relative magnitude of the Ohmic current and the displacement current, the magnitude of the magnetic field will get adjusted. If τ is small compared to τ_e, we are

in the transient region with respect to electric field and the displacement current will be larger than the Ohmic conduction current. In this case there will be nonzero magnetic field. In other case if τ is very large compared to τ_e, we are in the region where electric field is steady. Ohmic conduction current will dominate the displacement current.

2.7 Electrical Forces

This section calculates the total electromagnetic force on a fluid element of volume V and having charge density ρ. Fluid is flowing through the volume with velocity $\mathbf{u}$. According to Lorentz force law, total force on a point charge having charge q and travelling with velocity $\mathbf{u}$ in an electric and magnetic field is given by

$$\mathbf{F} = q\left(\mathbf{E} + \mathbf{u} \times \mathbf{B}\right)$$

Hence the total force on a fluid element is

$$\mathbf{F} = \int \rho\left(\mathbf{E} + \mathbf{u} \times \mathbf{B}\right) dV = \int \left(\rho\mathbf{E} + \mathbf{J} \times \mathbf{B}\right) dV = \int \mathbf{f} dV$$

where $\mathbf{f}$ is the force per unit volume. Using first and fourth Maxwell's equations

$$\mathbf{f} = \epsilon_0 \left(\nabla \cdot \mathbf{E}\right) \mathbf{E} + \left(\frac{1}{\mu_0} \nabla \times \mathbf{B} - \epsilon_0 \frac{\partial \mathbf{E}}{\partial t}\right) \times \mathbf{B} \tag{2.9}$$

Using the identity

$$\frac{\partial}{\partial t}\left(\mathbf{E} \times \mathbf{B}\right) = \left(\frac{\partial \mathbf{E}}{\partial t} \times \mathbf{B}\right) + \left(\mathbf{E} \times \frac{\partial \mathbf{B}}{\partial t}\right)$$

According to Faraday's law,

$$\frac{\partial \mathbf{B}}{\partial t} = -\nabla \times \mathbf{E}$$

Hence

$$\frac{\partial \mathbf{E}}{\partial t} \times \mathbf{B} = \frac{\partial}{\partial t}\left(\mathbf{E} \times \mathbf{B}\right) + \mathbf{E} \times \left(\nabla \times \mathbf{E}\right) \tag{2.10}$$

Substituting equation (2.10) in equation (2.9) gives

$$\mathbf{f} = \epsilon_0 \left[\left(\nabla \cdot \mathbf{E}\right) \mathbf{E} - \mathbf{E} \times \left(\nabla \times \mathbf{E}\right)\right] - \frac{1}{\mu_0} \left[\mathbf{B} \times \left(\nabla \times \mathbf{B}\right)\right] - \epsilon_0 \frac{\partial}{\partial t}\left(\mathbf{E} \times \mathbf{B}\right)$$

Using the product rule

$$\nabla\left(E^2\right) = 2\left(\mathbf{E} \cdot \nabla\right) \mathbf{E} + 2\mathbf{E} \times \left(\nabla \times \mathbf{E}\right)$$

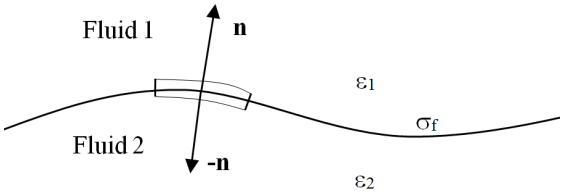

FIGURE 2.2: Interface between two fluids. σ_f is interfacial charge density

So

$$\mathbf{E} \times (\nabla \times \mathbf{E}) = \frac{1}{2}\nabla \left(E^2\right) - (\mathbf{E} \cdot \nabla)\,\mathbf{E}$$

Assuming steady state and the magnitude of magnetic field to be negligible as compared to that of electric field, the force per unit volume reduces to

$$\mathbf{f} = \epsilon_0 \left[(\nabla \cdot \mathbf{E})\,\mathbf{E} + (\mathbf{E} \cdot \nabla)\,\mathbf{E}\right] - \frac{1}{2}\epsilon_0 \nabla \left(E^2\right)$$

Defining a stress tensor T such that

$$T_{ij} = \epsilon_0 \left(E_i E_j - \frac{1}{2}\delta_{ij} E^2\right)$$

Hence

$$\mathbf{f} = \nabla \cdot \mathbf{T}$$

So the total force on a fluid element is given by

$$\mathbf{F} = \int \nabla \cdot \mathbf{T} dV$$

Hence the total stress acting on a fluid in the bulk is given by

$$\mathbf{T} = -p\mathbf{I} + \mu \left(\nabla \mathbf{u} + \nabla \mathbf{u}^T\right) + \epsilon_0 \left(\mathbf{E}\mathbf{E} - \frac{1}{2}\mathbf{I}E^2\right)$$

2.8 Boundary Conditions at the Interface

In this section, the connection of electrostatic and mechanical entities is established at the interface between two fluids.

2.8.1 Electric Field and Potential at the Interface

Consider figure 2.2.
Discontinuity of electric field at the interface is given by following framework.

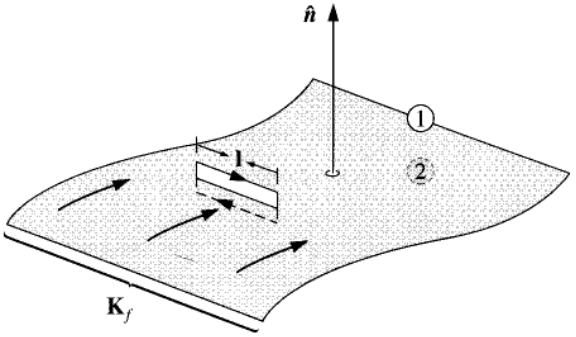

FIGURE 2.3: Contour for line integral across the interface [20]

Integrating 1^{st} Maxwell's equation gives

$$\int \mathbf{D} \cdot \mathbf{dS} = Q_{inside}$$

Applying this equation to the tiny wafer-thin Gaussian pillbox in the figure 2.2, extending slightly into the material on each side of the boundary,

$$\mathbf{D}_1 \cdot \mathbf{n} - \mathbf{D}_2 \cdot \mathbf{n} = \sigma_f a$$

where $\mathbf{D}$ is the electric displacement vector, σ_f is the interfacial charge density and a is the surface area of the Gaussian box. In the limit of zero box thickness,

$$\mathbf{D}_1{}^n - \mathbf{D}_2{}^n = \sigma_f$$

where $\mathbf{D}^n$ is the normal component of the electric displacement vector. In terms of electric fields, the equation reduces to

$$\epsilon_1 \mathbf{E}_1{}^n - \epsilon_2 \mathbf{E}_2{}^n = \sigma_f \tag{2.11}$$

This gives the relationship between the normal components of electric fields between two media.
Now integrating the 3rd Maxwell's equation gives

$$\int (\nabla \times \mathbf{E}) \cdot \mathbf{n} dS = -\frac{\partial}{\partial t} \int \mathbf{B} \cdot \mathbf{n} dS = 0 \tag{2.12}$$

Using the vector reformulation of Green's theorem (special case of Stokes' theorem)

$$\int (\nabla \times \mathbf{E}) \cdot \mathbf{n} dS = \oint \mathbf{E} \cdot \mathbf{t} dl$$

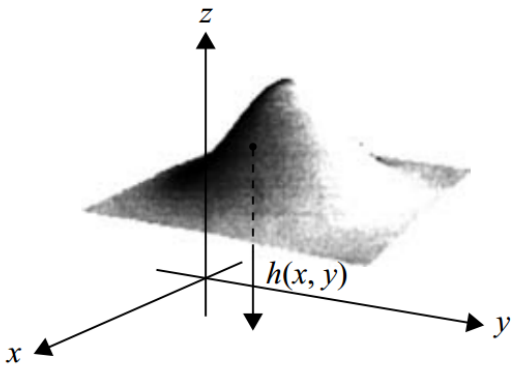

FIGURE 2.4: Coordinate system for locating the interface [20]

which is the relationship between surface integral and line integral. $\mathbf{t}$ is the unit vector in the tangential direction. Substituting above equation in equation (2.12) gives

$$\oint \mathbf{E} \cdot \mathbf{t} dl = 0$$

Referring to the figure 2.3 , the line integral over a loop reduces to

$$\mathbf{E}_1{}^t - \mathbf{E}_2{}^t = 0 \tag{2.13}$$

where $\mathbf{E}_t$ is the tangential component of the electric field E. This means that the components of the electric field parallel to the boundary are continuous.
The electric potential is always continuous at the interface. Otherwise the electric field at the interface would be infinite after the assumption that the interface thickness tends to zero.

$$\phi_1 - \phi_2 = 0 \tag{2.14}$$

2.8.2 Velocities at the Interface

As long as there is no mass transfer at the interface, velocity fields in fluids 1 and 2 are continuous at the interface. The continuity of tangential velocity is given below.

$$\mathbf{u}_1 \cdot \mathbf{t} = \mathbf{u}_2 \cdot \mathbf{t} \tag{2.15}$$

where $\mathbf{u}_1$ and $\mathbf{u}_2$ are the velocities of fluids 1 and 2 at the interface and $\mathbf{t}$ is the unit vector in the tangential direction. This is also known as *the no-slip condition.*
Since the interface is in motion, there should be a direct relationship between the shape of the interface and the normal components of the velocity fields at the interface. The

shape of the interface can be described by $F(x, y, z, t) = 0$. We can introduce a Cartesian coordinate system with x and y in the plane of the interface and z normal to it. Referring to figure 2.4, F can be given as

$$F = z - h\,(x, y, t) \qquad \forall x, y$$

The normal to the interface can be given as

$$\mathbf{n} = \pm \frac{\nabla F}{|\nabla F|}$$

Since $F = 0$ on the interface at all times, its substantial derivative should also be zero. That is

$$\frac{dF}{dt} = \frac{\partial F}{\partial t} + \mathbf{u} \cdot \nabla F = 0$$

Here the velocity $\mathbf{u}$ is that of interface. Rearranging gives

$$\frac{1}{|\nabla F|} \frac{\partial F}{\partial t} + \mathbf{u} \cdot \mathbf{n} = 0$$

So the kinematic boundary condition at the interface for the normal component of the velocity can be given as

$$\mathbf{u}_1 \cdot \mathbf{n} = \mathbf{u}_2 \cdot \mathbf{n} = -\frac{1}{|\nabla F|} \frac{\partial F}{\partial t} \tag{2.16}$$

If the interface is not moving, then the boundary condition at the interface reduces to

$$\mathbf{u}_1 \cdot \mathbf{n} = \mathbf{u}_2 \cdot \mathbf{n} = 0$$

2.8.3 Equilibrium of Forces at the Interface

For motions involving single fluid and solid boundaries, no slip and kinematic boundary conditions are sufficient to evaluate the complete solution of the equation of motion if the motion of boundaries is specified. However if the system involves interface between two fluids flowing, above conditions are not sufficient since they only give us the relationships between the velocity components which are all unknowns. So the additional conditions necessary to completely determine the velocity fields and the interface shape come from the equilibrium of forces at the interface. The argument is that since we have assumed the interface to be having zero thickness, its volume and hence mass is zero. So to avoid infinite acceleration, the net force on the interface due to surroundings should sum to zero.

According to Cauchy's theorem on stress tensor, the force per unit area on a surface is given by

$$\mathbf{f} = \mathbf{n} \cdot \mathbf{T}$$

where, $\mathbf{n}$ is the normal to the surface pointing outwards and $\mathbf{T}$ is the stress tensor acting on the surface.

In addition to viscous and electrical stresses, stress due to interfacial tension also needs to be considered. Interfacial tension contributes to the stress normal to the surface and not to the stress in tangential direction unless there is a gradient of interfacial tension. Let us consider an area A having arbitrary shape with $\mathbf{n}$ as the unit normal at each point and C as the closed curve enclosing area A. Let $\mathbf{t}$ be the unit vector normal to the curve C i.e. tangential to area A or the interface at each point. Then the stress balance condition is written as

$$\int_A \mathbf{n} \cdot [\mathbf{T}_1 - \mathbf{T}_2]\, dA + \int_C \gamma \mathbf{t} dl = 0$$

where the stress tensor $\mathbf{T}$ consists of viscous and electrical stress tensors.

$$\mathbf{T} = -p\mathbf{I} + \mu\left(\nabla\mathbf{u} + \nabla\mathbf{u}^T\right) + \epsilon_0\left(\mathbf{E}\mathbf{E} - \frac{1}{2}\mathbf{I}|\mathbf{E}|^2\right)$$

Converting the line integral into surface integral using Stokes' law gives

$$\int_C \gamma \mathbf{t} dl = \int_A \nabla_s \gamma dA - \int_A \gamma \mathbf{n}\left(\nabla \cdot \mathbf{n}\right) dA$$

where, $\nabla_s = \nabla - \mathbf{n}(\mathbf{n} \cdot \nabla)$ is the component of the gradient operator in the local plane of the interface. We remove the component of the gradient normal to the surface. Combining equations gives

$$\int_A \left(\mathbf{n} \cdot [\mathbf{T}_1 - \mathbf{T}_2] + \nabla_s \gamma - \gamma \mathbf{n}\left(\nabla \cdot \mathbf{n}\right)\right) dA = 0$$

It can be shown that the integrand is zero at each point on the interface since the interfacial element chosen is of arbitrary shape and the integrand is a continuous function of the position on the interface. Hence

$$\mathbf{n} \cdot [\mathbf{T}_1 - \mathbf{T}_2] + \nabla_s \gamma - \gamma \mathbf{n}\left(\nabla \cdot \mathbf{n}\right) = 0$$

The term $\nabla \cdot \mathbf{n}$ is defined to be the curvature of the interface and is given by

$$\nabla \cdot \mathbf{n} = \left(\frac{1}{R_1} + \frac{1}{R_2}\right) = 2H$$

Here, R_1 and R_2 are the principle radii of curvature of the interface.

So the jump condition of stress at the interface can be given as

$$\mathbf{n} \cdot [\mathbf{T}_1 - \mathbf{T}_2] = 2H\gamma\mathbf{n} - \nabla_s \gamma \tag{2.17}$$

2.8.3.1 Tangential Stress Balance

The interfacial tension contributes to the tangential component of the stress only through its surface gradient. If interfacial tension is assumed to be constant in magnitude with respect to space, the stress due it will be zero which implies that there is no jump in the stress tensor and hence stress tensor in continuous at the interface. Following is the general equation for the stress balance in the tangential direction.

$$\mathbf{n} \cdot [\mathbf{T}_1 - \mathbf{T}_2] \cdot \mathbf{t} + \nabla_s \gamma = 0 \tag{2.18}$$

2.8.3.2 Normal Stress Balance

The stress balance in the normal direction is given by taking the dot product of equation (2.17) with unit normal to the interface.

$$\mathbf{n} \cdot [\mathbf{T}_1 - \mathbf{T}_2] \cdot \mathbf{n} - 2H\gamma\mathbf{n} = 0 \tag{2.19}$$

Chapter 3

Electro-coflow Simulation

Physical Description of the Problem

The figure 3.1 shows an axisymmetric system consisting of cylindrical tank of dimensionless radius $R_2 = 5$. The tank contains two immiscible and incompressible fluids co-flowing in which fluid 1 is injected from the right side of the tank via the electrode nozzle having dimensionless radius $R_1 = 1$. Both fluids are injected with fully developed dimensionless velocity profile $v_i = 2\left(1 - (R/R_i)^2\right)$. Fluid 1 is assumed to be leaky dielectric and highly conducting compared to fluid 2.

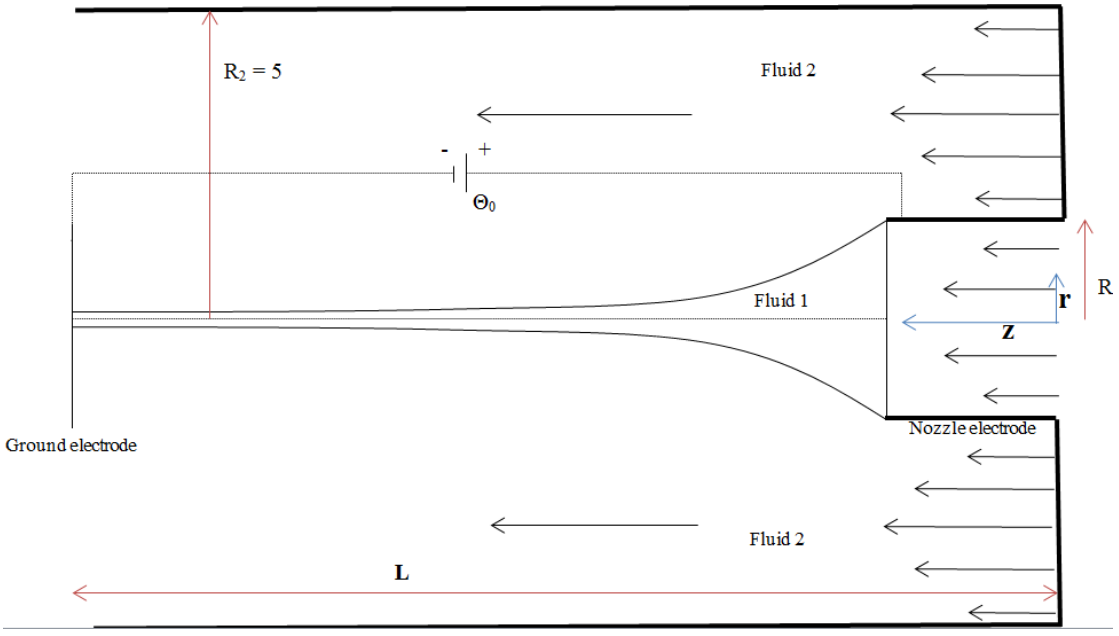

FIGURE 3.1: System of interest

An electric potential is applied between a metallic grounded electrode at the left and a nozzle. **L** is the length of the jet of inner liquid before it hits the metallic counter-electrode or breaks. Fluid 1 which is inner liquid is taken to be reference fluid. Since inner fluid is a leaky dielectric, the current resulted from it consists of contributions from the conduction and convection current from its bulk as well as surface. Outer fluid is assumed to be perfect dielectric and polarization of its medium is assumed to be negligible. Electric permittivities, mass densities and viscosities of fluids 1 and 2 are ϵ_1 and ϵ_2 ($\epsilon_1 > \epsilon_2$), ρ_1 and ρ_2 and μ_1 and μ_2 respectively. K_1 and K_2 are electric conductivities of the fluids 1 and 2 respectively. All properties of materials are assumed to be constant throughout the process. Edge effects can be neglected. Our goal is to find the solution for velocity, electric potential and pressure fields for the cone-jet mode and to track the interface motion during the dynamic simulation. The radial velocity is u while the axial velocity is v. Effect of gravity is neglected. The non-dimensionalization takes R_1 as characteristic length, capillary velocity $u_c = \sqrt{\gamma/R_1\rho_1}$ as characteristic velocity and potential difference between two electrodes Θ_0 as characteristic potential difference.
Following are the boundary conditions for the present problem:

For $z = 0$; $0 < r < R_1 \rightarrow u = 0, v = V_1, \Theta = \Theta_0$

For $z = 0$; $R_1 < r < R_2 \rightarrow u = 0, v = V_2, \partial\Theta/\partial z = 0$

For $z = L$; $0 < r < R_2 \rightarrow \partial u/\partial z = 0, \partial v/\partial z = 0, \Theta = 0$

For $r = 0$; $0 < z < L \rightarrow u = 0, \partial v/\partial r = 0, \partial\Theta/\partial r = 0$

For $r = R_2$; $0 < z < L \rightarrow u = 0, v = 0, \partial\Theta/\partial r = 0$

3.1 Modelling Interface Dynamics - A Level Set Approach

This approach has been designed specifically for analysing interface dynamics in multi-phase flows. We can represent a single phase fluid flow by modelling the flow-properties such as velocity, pressure using Navier-Stokes equations. However in case of a multi-fluid flow, the motion of an interface which is induced by the fluid flow also needs to be represented and modelled mathematically for a Computational Multi-Fluid Dynamics simulation. The primary interface tracking techniques for simulating a separated two phase flow are based on front tracking, volume of fluid (VOF) method and the level set method (LSM). Here the level set method will be discussed in detail.

LSM was first proposed by Osher and Sethian [21] as an Eulerian computational technique of capturing moving interfaces and shapes. Apart from computational fluid dynamics, this method also has a place as a useful numerical technique in material science, computer vision and computational geometry. The first use of LSM for solving a problem of incompressible two-phase flow was done by Sussman [22]. They introduced a new approach of dealing with such systems called "single-field formulation". In this approach, the individual fluids within the system lose their identity and entire system of fluids is considered as single specie with variable fluid properties. One set of equations for conservation of mass, momentum and charge are written for the entire flow field. Interfacial source terms such as force due to surface tension, interfacial charge are added along with delta functions that are non-zero only at the interface. It should be noted that away from the interface, the single field formulation reduces to the customary mass, momentum and charge conservation equations for each of the bulk fluids while at the interface the formulation naturally incorporates the correct mass, momentum and charge balance across the interface. Suitable interpolating function for varying fluid properties is used at the interface. The level set function is used to represent the region occupied by different fluids. In this method, since fluid properties do not change across the interface, a small finite margin is assumed across which the properties vary according to some function. Since this margin is finite, this method is also called "the diffused interface method". Consequently all the interfacial forces are modelled as volumetric forces with some criteria which will be discussed later. The volumetric source term of the surface tension force was firstly derived and added to the Navier-Stokes equation by Chang [23]. The level set method, as compared to the volume of fluid method, is easier to implement numerically and describes the interfacial information i.e. normal, curvature, location more accurately. The major disadvantage of this method is the mass error occurring due to the diffused nature of the interface. Attempts have been made in improving LSM by reducing this error. A level set method-based immersed boundary method was introduced by Son [24] for solving problems involving complex domains using Cartesian grids. Son and Hur [25] simulated a motion of droplets over an inclined plane by presenting a method of modelling the contact angle which was combined with an immersed boundary based level set method. Furthermore, Suh and Son [26] modelled three fluid interaction using level set method and simulated a thermal inkjet process.
It can be said that the level set method is one of the most popular and recent methods in order to simulate two-phase flow in addition to different applications in other disciplines of science and engineering. Following section introduces this method.

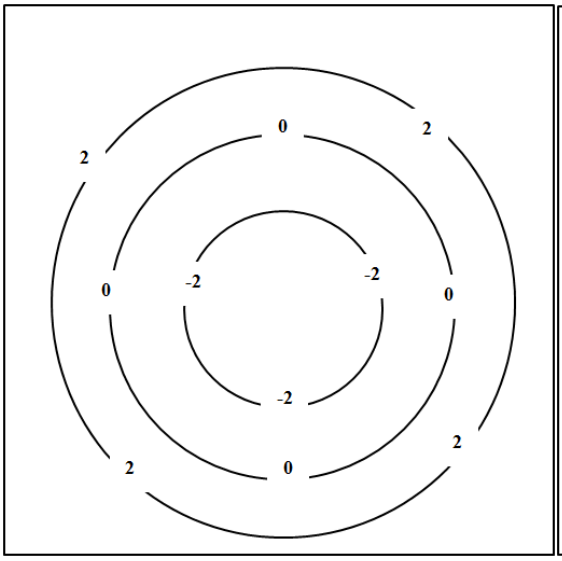

FIGURE 3.2: ϕ Contours

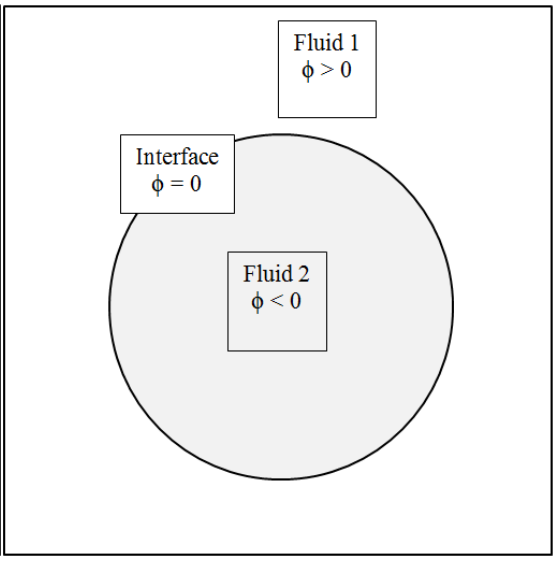

FIGURE 3.3: Interface representation

3.1.1 Functions used in the level set method

The level set method is an Eulerian computational method which captures moving interfaces or boundaries and is comprised of three methods viz. a level set function which defines the interface, a Heaviside function which calculates which is used as an interpolating function across diffused interface to calculate fluid properties, an a Dirac delta function for modelling the effect of surface tension force and electric force (modelled as volumetric forces) in Navier-Stokes equations.

3.1.1.1 Level Set Function

The idea of implicit surfaces has been used as a basis for representing the interface via level set function, wherein a level set function $\phi = 0$ is defined in a domain having a fixed value at the interface. We define the level set function to be the signed normal distance function measured from the interface and it is equal to zero at the interface. Figure 3.3 shows a circular interface having a radius of 5 units and the level set function $\phi = 0$ at the interface along with positive values in fluid 1 and negative values in fluid 2. Figure 3.2 shows the contour plots of the level set function for this interface as concentric circles with increasing absolute value with their normal distance from the interface i.e. as they move away from the interface. The level set field is defined to be smooth and exact position of the interface at any instant can be captured by locating the level set function having a value zero. This framework of finding the interface position avoids the logical difficulties which we encounter while constructing the interface.

3.1.1.2 Heaviside Function

In a single field formulation, the Navier-Stokes equations consider individual material properties in different fluids and weighted properties at the interface. In the whole computational domain, the fluid density and the viscosity can be calculated as

$$\rho_m = \rho_1 H(\phi) + \rho_2[1 - H(\phi)] \tag{3.1}$$

$$\mu_m = \mu_1 H(\phi) + \mu_2[1 - H(\phi)] \tag{3.2}$$

where the mean, fluid 1 and fluid 2 are represented by the subscripts m, 1 and 2 respectively and $H(\phi)$ is a Heaviside function defined as

$$H(\phi) = \begin{cases} 1, \text{ if } \phi > 0 \\ 0.5, \text{ if } \phi = 0 \\ 0, \text{ if } \phi < 0 \end{cases} \tag{3.3}$$

We can define the volume occupied by fluid 1 in a representative control volume P of volume Δ as

$$\Delta V_1 = \int_{\Delta V_P} H(\phi) dV$$

The value of the Heaviside function $H(\phi)$ at the centroid of the control volume can be used as an approximation of its volume averaged value, using the second order approximation technique, i.e.

$$\Delta V_1 = \overline{H(\phi)} \Delta V_P \approx H(\phi_P) \Delta V_P$$

Thus, we can express the Heaviside function at the centroid of the control volume as

$$H_P = H(\phi_P) \approx \frac{\Delta V_1}{\Delta V_P} = \frac{\text{Volume of fluid 1 in a CV}}{\text{Volume of a CV}} \tag{3.4}$$

This is interpreted physically as the volume fraction used in the volume of fluid method. In this method, the VOF function is geometrically initialized using equation (3.4) and it requires a special treatment while evolving the VOF field in order to maintain its step discontinuity with time.

Also, the expression for calculating the surface area occupied by fluid 1 on a face f (east/west/south/north face in a control volume) can be proposed as

$$\Delta S|_{1,f} = \int_{\Delta S_f} H(\phi) dS$$

Similarly, we can use a second order approximation and approximate the surface-averaged value of the Heaviside function $H(\phi)$ at the face of a control volume by its

value at the face center i.e.

$$\Delta S_{1,f} = \overline{H(\phi)}\Delta S_f \approx H(\phi_f)\Delta S_f$$

Thus we can express the Heaviside function at the face center f of a CV as

$$H_f = H(\phi_f) \approx \frac{\Delta S_{1,f}}{\Delta S_f} = \frac{\text{Surface area occupied by fluid 1 on a face}}{\text{Surface area of a face}} \tag{3.5}$$

This can be explained physically as area function. For example in a control volume, in the leftmost figure in figure 3.6, $H_e = 0$, $H_w = 1$, $H_n > 0.5$, and $H_s < 0.5$. The above equation needs H_f to be calculated geometrically. However, in the level set method, we define the Heaviside function at the cell center and interpolate the neighbouring cell center values to calculate the value at the face center H_f.

As a short summery about the Heaviside function, the Heaviside function is non-dimensional and the physical interpretation of its value at the centroid of the control volume is the fraction of the total volume occupied by the fluid 1 in the control volume. Also, its value at the face center of the control volume can be explained as fraction of the face area occupied by fluid 1. The equations are going to be used while deriving the governing equations for the level set function. It should be noted the finite volume method commonly uses the second-order approximation for volume and surface averaging used above for physical explanation of the Heaviside function at the cell and face centers respectively.

However, in the level set method the sharp nature of the Heaviside function calculated from equation (3.5) results in an unstable numerical solution. Hence we need to avoid geometrically calculating the volume of fluid 1 in the control volume using equation (3.4). Therefore we use a smoothed version of Heaviside function which results in its continuous variation across the interface. The function is defined as follows:

$$H_\epsilon(\phi) = \begin{cases} 0, \text{ if } \phi < -\epsilon \\ \frac{\phi+\epsilon}{2\epsilon} + \frac{1}{2\pi}\sin\left(\frac{\pi\phi}{\epsilon}\right), \text{ if } |\phi| < \epsilon \\ 1, \text{ if } \phi > \epsilon \end{cases} \tag{3.6}$$

The above expression for the Heaviside function implies that the nature of the interface is diffused. It has a finite thickness 2ϵ and the variations in all fluid properties are smoothed across this domain. It should be noted that we have defined the interface thickness to always be normal to the interface (which is represented as $\phi = 0$) and the corresponding level set function for the interface thickness is bounded as $-\epsilon \leq \phi \leq \epsilon$, where we define ϵ as some factor of the spacing between the grids. A standard factor of 3/2 is generally used while defining ϵ ($2\epsilon = 3\Delta x$), which supports the argument that the

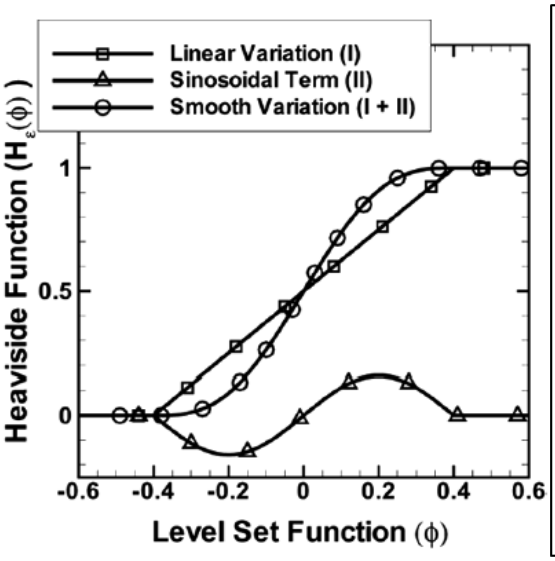

FIGURE 3.4: Smoothed Heaviside function [27]

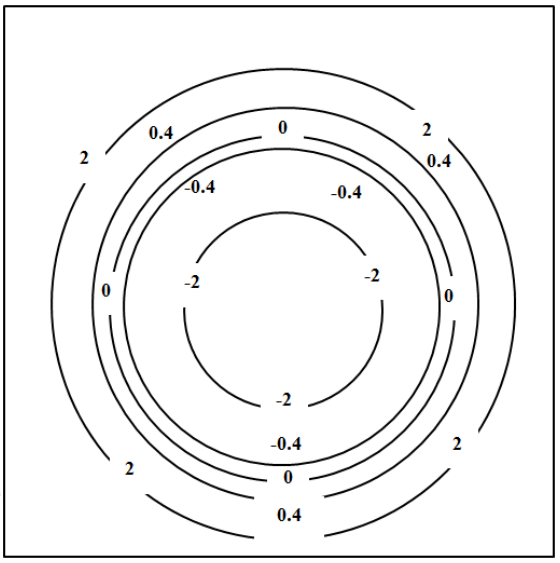

FIGURE 3.5: Level set contours with interface thickness

as we refine the grid, the interface thickness will become narrower and will be negligible on fairly fine grid. It should be understood that the only physically relevant interface is $\phi = 0$. The values of the level set functions inside the interface thickness are only useful for smoothening the variation in the fluid property across the interface. In this way, the values of level set function outside the interface thickness do not have any role in the numerical model.

Figure 3.5 shows an interface thickness i.e. diffused interface of width of 0.8 units for a circular interface of radius 5 units. Equation (3.6) for a Heaviside function applicable within the interface thickness includes two terms viz. the linear term which varies from 0 to 1 and a sinusoidal term. The behaviours of both terms inside the diffused interface have been shown in figure 3.4. We see that the linear term changes its gradient abruptly at the boundaries of the interface thickness and adding the sinusoidal term to the linear term smoothens the function at the boundaries and the slope of the Heaviside function H_ϵ varies continuously across the diffused interface. We can observe that the value of the Heaviside function at the actual interface position $\phi = 0$ is 0.5. This implies that the fluid property at the interface is an arithmetic mean of individual properties of two fluids. Also, the integral of H_ϵ i.e. the area under the smoothly varying curve in figure 3.4 within the interface thickness is 0.5. This value is same as the value of the Heaviside function if it is assumed to vary sharply across the diffused interface like equation (3.3). As we refine the grid, the smoothed Heaviside function evaluated according to equation (3.6) behaves like a sharp Heaviside function (equation (3.3)).

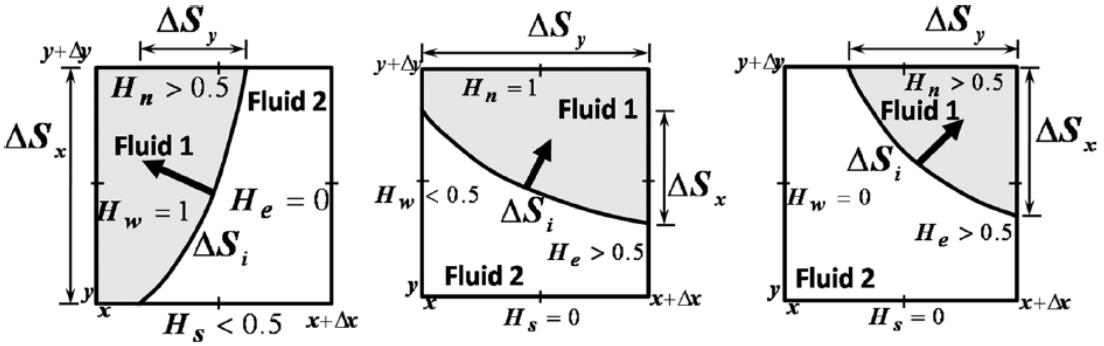

FIGURE 3.6: Control volume with elemental interface shown in terms of its components with the values of Heaviside function at the face centers [27]

3.1.1.3 Dirac Delta Function

The Dirac delta function is used to model the interfacial entities as the volumetric source terms [1,2]. For a level set function field, the Dirac delta function can be defined using the Heaviside function as

$$\delta(\phi) = \frac{dH(\phi)}{d\phi} \tag{3.7}$$

In order to physically interpret the Dirac delta function, the interfacial area (ΔS_i) needs to be calculated accurately using the Heaviside function. Consider figure 3.6 which shows an elemental interface in an infinitesimal control volume. We can express the magnitude of the surface area ΔS_i in the control volume as

$$\Delta S_i = (\Delta S_x \hat{i} + \Delta S_y \hat{j}) \cdot \hat{n}(\phi)$$

where

$$\Delta S_x = (H\Delta y)_{x+\Delta x} - (H\Delta y)_x$$

$$\Delta S_y = (H\Delta x)_{y+\Delta y} - (H\Delta x)_y$$

are the components of the vector representing the interfacial area in x and y directions, respectively, with the use of the Heaviside function at the face centers of the control volume (equation 3.5). $\hat{n}(\phi)$ is the unit vector normal to the interface. Both the expressions for ΔS_x and ΔS_y are substituted in the expression for ΔS_i, both sides are divided by the volume of the CV which is $\Delta V = \Delta x \Delta y$ and the limits for $\Delta x, \Delta y \to 0$ are taken. This gives us the ratio of the surface area of the interface to the volume of the CV as

$$\frac{\Delta S_i}{\Delta V} = \nabla H \cdot \hat{n}(\phi) = \frac{\partial H}{\partial \phi} \equiv \delta(\phi) \tag{3.8}$$

where $\nabla H \cdot \hat{n}(\phi) = (\partial H/\partial\phi) \cdot \hat{n} = \partial H/\partial\phi$ with the unit normal vector $\hat{n} = \nabla\phi/|\nabla\phi|$ and $|\nabla\phi| = 1$ as the level set function is the normal distance function. Thus, the unit

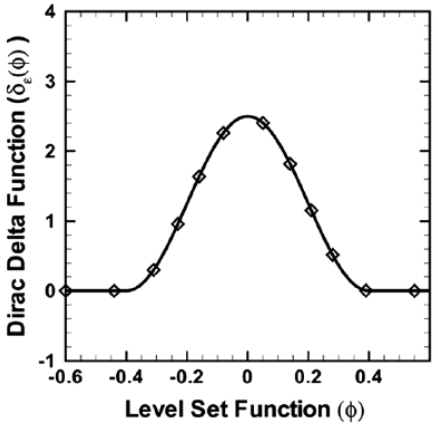

FIGURE 3.7: Smoothed Dirac Delta function [27]

of the Dirac delta function is m^{-1} and its physical interpretation is the interfacial area of the CV to the volume of the CV. The Dirac delta function is non-zero only at the interface i.e. $\phi = 0$. But the Dirac delta function calculated via this method i.e. in the context of the level set method is a smoothed version which is calculated from equations (3.6) and (3.7) as

$$\delta_\epsilon(\phi) = \frac{\partial H}{\partial \phi} = \begin{cases} \frac{1}{2\epsilon}\left(1 + \cos\left(\frac{\pi\phi}{\epsilon}\right)\right), & \text{if } |\phi| < \epsilon \\ 0, & \text{otherwise} \end{cases} \tag{3.9}$$

As can be seen from figure 3.7, the smoothed Dirac delta function decreases symmetrically about $\phi = 0$, across the interface thickness. Also, the integral of δ_ϵ i.e. the area under the curve of in figure 3.7 within the interface thickness comes out to be 1. With the grid refinement, the smoothed Dirac delta function which is evaluated numerically using equation (3.9), tends to coincide with the sharp Dirac delta function, which is calculated geometrically using equation (3.8).

3.1.2 Governing equations for the level set function

In Computational-Electro-MultiFluid-Dynamics (CEMFD), we use the governing equations for velocities and pressure as Navier-Stokes equations, charge conservation equation for governing the charge distribution and governing equations for the level set function for the temporal evolution of the interface. This way, there are four variables, velocity, pressure, charge and the level set function and three conservation laws; for mass, momentum and charge. Therefore, one more conservation law has to be invoked and this can be done by making use of the fluid properties in the system that both fluids are incompressible and their properties remain constant with time.

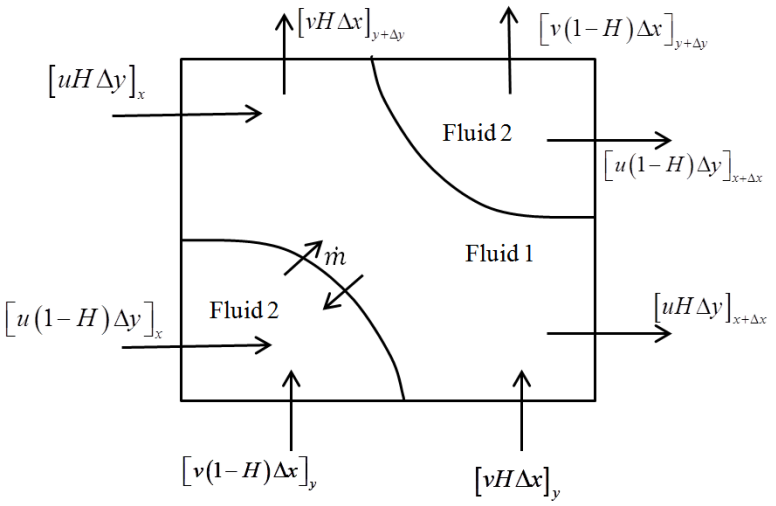

FIGURE 3.8: Control volume representation where both fluids flow through all the faces for volume conservation equation

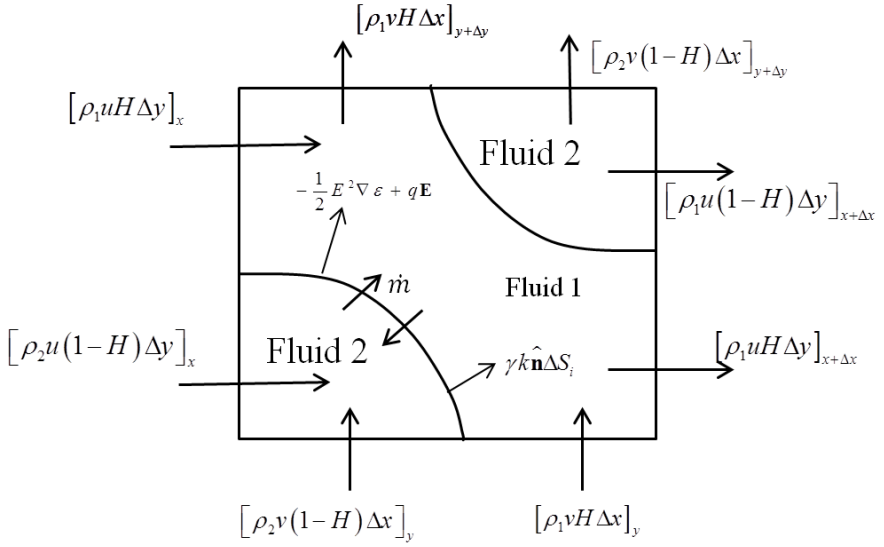

FIGURE 3.9: Control volume representation where both fluids flow through all the faces for mass conservation equation. Forces corresponding to surface tension and electrostatics (considering leaky dielectric fluids) are also shown.

3.1.2.1 Volume Conservation Equation

In the case of a control volume filled with both fluids 1 and 2 which are incompressible in nature, the volume of an individual phase can change if there is a mass transfer across the interface via phase change or transport of chemical species but the total volume of both fluids comprising the CV cannot change.

This section proves the continuity equation using the incompressible condition of both phases and zero mass transfer across the interface. Consider figure 3.8 showing a Cartesian control volume with width Δx and Δy and partly occupied by two fluids with ΔS_i as the total interfacial area. Let the interfacial mass flux be $\dot{m}$.

We can write the statement for the conservation of volume for the control volume as

(Rate of increase of volume) = (Rate of volume in) – (Rate of volume out) + (Rate of volume generation)

According to the assumption of the single field formulation done earlier, we have defined a single velocity field in which u and v are velocity components in x and y directions respectively. As seen in figure 3.8, interface is passing through all the faces of the control volume and both fluids flow across it. As compared to the control volume in this figure, control volumes with just one interface separating two fluids are more common since the size of the control volume is very small. But the control volume in figures 3.8 and 3.9 is a more generalized form and hence is used for the derivation of the continuity equation. Using equation (3.5), we can calculate the surface area occupied by each fluid on all faces of the control volume. Thus, the product of velocity normal to the control volume and the surface area represents the total volumetric flow rate of a fluid on a partly occupied face of the control volume as shown in figure 3.8. As an example, the rates of volume of fluids 1 and 2 leaving the top horizontal face of the control volume are $vH\Delta x$ and $v(1-H)\Delta x$ respectively. The figure shows similar expressions for other fluxes. We can calculate the individual volumes occupied by fluid 1 and 2 using equation (3.4) as $H_p\Delta x\Delta y$ and $(1-H_p)\Delta x\Delta y$, respectively, due to interfacial mass flux, the rates of generation of volumes of fluids 1 and 2 are $-\dot{m}\,\Delta S_i/\rho_1$ and $\dot{m}\,\Delta S_i/\rho_2$ respectively. Balancing the volume can then be reformulated as

$$\frac{\partial\left(H_P\Delta x\Delta y\right)}{\partial t}+\frac{\partial\left((1-H_P)\Delta x\Delta y\right)}{\partial t}=$$

$$\Delta y\left[(uH)_x-(uH)_{x+\Delta x}\right]+\Delta y\{[u\,(1-H)]_x-[u\,(1-H)]_{x+\Delta x}\}$$

$$+\Delta x\left[(vH)_y-(vH)_{y+\Delta y}\right]+\Delta x\{[v\,(1-H)]_y-[v\,(1-H)]_{y+\Delta y}\}+\dot{m}\,\Delta S_i\left(\frac{1}{\rho_2}-\frac{1}{\rho_1}\right)$$

Since we have assumed both fluids to be incompressible, the left hand side of the above equation should be zero. Now, whole equation is divided by $\Delta V=\Delta x\Delta y$ and limits for $\Delta x,\Delta y\to 0$ are taken. Then we use the definition of partial derivatives and arrive at

$$\nabla\cdot\mathbf{u}=\dot{m}\,\frac{\Delta S_i}{\Delta V}\left(\frac{1}{\rho_2}-\frac{1}{\rho_1}\right)=\left(\frac{1}{\rho_2}-\frac{1}{\rho_1}\right)\vec{m}\cdot\nabla H=\left(\frac{1}{\rho_2}-\frac{1}{\rho_1}\right)\dot{m}\,\delta(\phi)$$

where $\vec{m}$ is interfacial mass flux vector and the expression for $\Delta S_i/\Delta V$ has been taken from equation (3.8).

Since we have assumed that the fluids are immiscible with each other, the interfacial mass flux vector becomes zero and we arrive at the continuity equation for incompressible

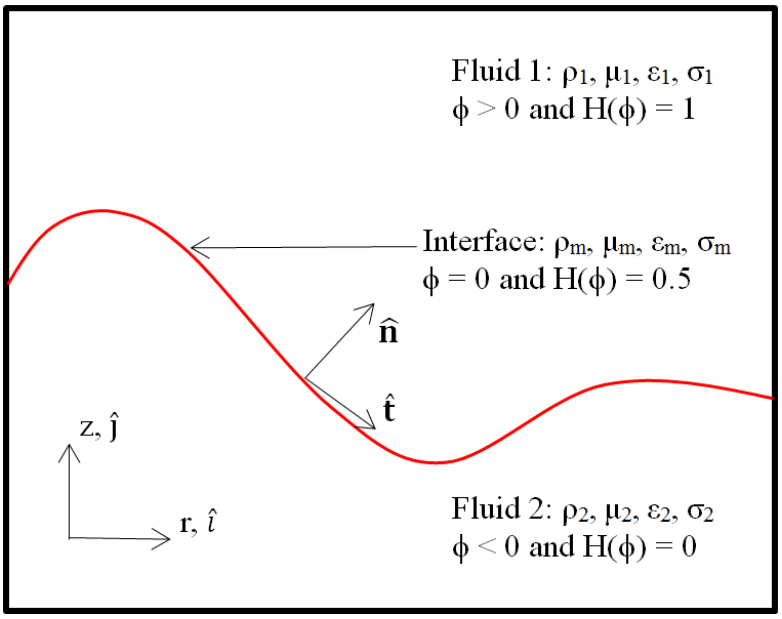

FIGURE 3.10: A representative 2-D axisymmetric electro-multifluid-dynamics system

and immiscible fluids as

$$\nabla \cdot \mathbf{u} = 0$$

Consider an axisymmetric two phase immiscible flow under the application of an electric field in the axial direction on the interface separating the two fluids. All thermophysical and electrical properties of both fluids are shown in the figure 3.10. The interface is assumed to be massless and can be tracked by the level set function $\phi = 0$. The continuity equation thus reduces for this system to

$$\frac{1}{R}\frac{\partial(RU)}{\partial R} + \frac{\partial V}{\partial Z} = 0$$

where the dimensionless variables are scaled as

$$U = \frac{u}{u_c}; V = \frac{v}{u_c}; R = \frac{r}{l_c}; Z = \frac{z}{l_c}$$

where l_c is taken to be the capillary radius and u_c as the capillary velocity: $u_c = \sqrt{\frac{\gamma}{\rho_2 l_c}}$.

3.1.2.2 Mass Conservation (Level Set Advection Equation)

For a control volume figure 3.9, we can write the mass balance as

(Rate of increase of mass) = (Rate of mass in) - (Rate of mass out)

Rate of mass flow across the face of the control volume can be represented as

the product of fluid density, the velocity normal to the face of the control volume and the surface area where we calculate the surface area for each fluid by the use of equation (3.5). The net mass balance then becomes as follows

$$\frac{\partial\left(\rho_1 H_P \Delta x \Delta y\right)}{\partial t} + \frac{\partial\left(\rho_2 (1-H_P) \Delta x \Delta y\right)}{\partial t} =$$
$$\Delta y\left[\left(\rho_1 u H\right)_x - \left(\rho_1 u H\right)_{x+\Delta x}\right] + \Delta y\{[u\left(\rho_2 1 - H\right)]_x - [u\left(\rho_2 1 - H\right)]_{x+\Delta x}\}$$
$$+\Delta x\left[\left(\rho_1 v H\right)_y - \left(\rho_1 v H\right)_{y+\Delta y}\right] + \Delta x\{[\rho_2 v\left(1-H\right)]_y - [\rho_2 v\left(1-H\right)]_{y+\Delta y}\}$$

After dividing the whole equation by $\Delta V = \Delta x \Delta y$, taking limits for Δx,$\Delta y \to 0$ and using the definition of partial derivatives we arrive at

$$\left(\rho_1 - \rho_2\right)\left(\frac{\partial H}{\partial t} + \overrightarrow{u} \cdot \nabla H\right) + \rho_m \nabla \cdot \overrightarrow{u} = 0 \tag{3.10}$$

where $\rho_m = \rho_1 H + \rho_2(1-H)$ is the mean fluid density at the interface according to equation (3.1). Second term in equation (3.10) becomes zero according to the continuity equation. Substituting the equation (3.1) in above equation gives the governing equation for the Heaviside function as an advection equation.

$$\frac{\partial H}{\partial t} + \overrightarrow{u} \cdot \nabla H = 0$$

Now the substitution $\partial H = \delta(\phi)\partial\phi$ is made using equation (3.7) and we get the governing equation for the level set function.

$$\frac{\partial \phi}{\partial t} + \overrightarrow{u} \cdot \nabla \phi = 0 \tag{3.11}$$

For the system in figure 3.10, equation (3.11) reduces to

$$\frac{\partial \phi}{\partial \tau} + U\frac{\partial \phi}{\partial R} + V\frac{\partial \phi}{\partial Z} = 0 \tag{3.12}$$

3.1.2.3 Subsidiary Equation: Re-initialization

The level set functions defined in this methodology are defined to be normal distance function fields, which means that the values of these functions are determined according to their distance along the normal with the interface level set function $\phi = 0$. However, after solving the mass conservation equation i.e. the advection equation (3.12), entire level set field will not remain as the normal distance function field. We need a constant thickness of the diffused interface along the interface at each time step in order to accurately calculate Heaviside function(eq. (3.6)) and Dirac delta function (eq. (3.9)). We ensure this by re-initializing the advected level set function field to a signed normal

distance function field. We do not alter the configuration of the interface function $\phi = 0$ which is obtained after the advection. In case of multi-phase flows, level set method re-initializes according to PDE-based formulation which changes the irregular level set function (ϕ_0) to a signed normal distance function by obtaining the steady state solution of

$$\frac{\partial \phi}{\partial t_s} + S_\epsilon(\phi_0)\left(|\nabla \phi| - 1\right) = 0 \tag{3.13}$$

where $S_\epsilon(\phi_0) = \phi_0 \Big/ \sqrt{{\phi_0}^2 + \epsilon^2}$ is the smoothed sign function. t_s is the pseudo time and has no relation with the system time coordinate t. The steady state solution of equation (3.13) is a normal distance function which can be mathematically ensured by $|\nabla \phi| = 1$. Equation (3.13) can be rearranged as

$$\frac{\partial \phi}{\partial t_s} + S_\epsilon(\phi_0)\widehat{n} \cdot \nabla \phi = S_\epsilon(\phi_0) \tag{3.14}$$

This is a hyperbolic equation with a characteristic advecting velocity as $S_\epsilon(\phi_0)\widehat{n}$. We see that since $S_\epsilon(\phi_0) = 0$ at the interface, the advection velocity is zero and is normal to the interface as we go away from the interface pointing away from the interface in both phases due to the sign function. The information about the interface is carried in the direction normal to the interface into both fluids by the advecting velocity field. The advantage of PDE-based formulation for re-initializing level set functions is that the normal distance function is recovered without needing the exact interface position.

3.1.2.4 Momentum Equations

In the absence of Marangoni effect driven by tangential gradient in the interfacial tension, the role of interfacial tension is to balance the jump of the normal stress across the interface and drive the interface towards the state of minimum area thus minimum interfacial energy. Tangential and normal force balances across the interface are given by equations (2.18) and (2.19) respectively as

$$\mathbf{n} \cdot [\mathbf{T}_1 - \mathbf{T}_2] \cdot \mathbf{t} + \nabla_s \gamma = 0$$

and

$$\mathbf{n} \cdot [\mathbf{T}_1 - \mathbf{T}_2] \cdot \mathbf{n} - \gamma \left(\nabla \cdot \mathbf{n}\right) \mathbf{n} = 0$$

where

$$\mathbf{T} = -p\mathbf{I} + \mu_m \left(\nabla \mathbf{u} + \nabla \mathbf{u}^T\right) + \epsilon_0 \left(\mathbf{E}\mathbf{E} - \frac{1}{2} I |\mathbf{E}|^2\right)$$

γ is the interfacial tension and the mean viscosity $\mu_m = \mu_1 H(\phi) + \mu_2[1 - H(\phi)]$ according to equation (3.2).

The notable aspect about the single field formulation assumed for solving the system of interest is that the interfacial force balance equations written above are satisfied implicitly by solving the Navier-Stokes equation in the complete domain consisting of both fluids by the use of volume-averaged properties. In this way, interfacial tension term and the term for the Maxwell stress are incorporated into Navier-Stokes equation as the source terms using the continuum surface force model of Brackbill [28]. The interfacial tension force vector for a control volume in figure 3.9 can be given as

$$\mathbf{F}_{ST} = \gamma\kappa\widehat{n}\Delta S_i$$

Interfacial area in this equation can be replaced in terms of Dirac delta function according to equation (3.8), and the expression for interfacial tension force per unit volume can be obtained as

$$\mathbf{F}_{ST}/\Delta V = \gamma\kappa\widehat{n}\delta(\phi)$$

where $\widehat{n}$ is the unit normal vector and κ is the interface curvature given as

$$\widehat{n} = \frac{\nabla\phi}{|\nabla\phi|} \Rightarrow \frac{\phi_R}{\sqrt{\phi_R^2+\phi_Z^2}}\widehat{i} + \frac{\phi_Z}{\sqrt{\phi_R^2+\phi_Z^2}}\widehat{j}$$

$$\kappa = -\left[\frac{\phi_Z^2\phi_{RR} - 2\phi_R\phi_Z\phi_{RZ} + \phi_R^2\phi_{ZZ} + \left(\phi_R \Big/ R\sqrt{\phi_R^2+\phi_Z^2}\right)}{\left(\phi_R^2+\phi_Z^2\right)^{3/2}}\right]$$

where the subscripts correspond to partial derivatives.

The source term for interfacial tension in Navier-Stokes equation can be substituted as this volumetric body force term according to single field formulation. The volumetric force term for Maxwell stress ($\mathbf{F}_{ES}$)is also modelled as a source term and its formulation will be discussed in detail in the next section.

Momentum conservation equation in the radial direction becomes

$$\frac{\partial(\rho_m U)}{\partial t} + \frac{1}{R}\frac{\partial(R\rho_m UU)}{\partial R} + \frac{\partial(\rho_m VU)}{\partial Z}$$

$$= -\frac{\partial P}{\partial R} + \frac{1}{\mathrm{Re}}\left[\frac{1}{R}\frac{\partial(R\tau_{rr})}{\partial R} + \frac{\partial\tau_{zr}}{\partial Z}\right] + \left(\frac{\mathbf{F}_{ST}}{We} + Bo_e\mathbf{F}_{ES}\right)\cdot\widehat{i} \tag{3.15}$$

Momentum conservation equation in the axial direction becomes

$$\frac{\partial(\rho_m V)}{\partial t} + \frac{1}{R}\frac{\partial(R\rho_m UV)}{\partial R} + \frac{\partial(\rho_m VV)}{\partial Z}$$

$$= -\frac{\partial P}{\partial Z} + \frac{1}{\mathrm{Re}}\left[\frac{1}{R}\frac{\partial(R\tau_{rz})}{\partial R} + \frac{\partial\tau_{zz}}{\partial Z}\right] + \left(\frac{\mathbf{F}_{ST}}{We} + Bo_e\mathbf{F}_{ES}\right)\cdot\widehat{j} \tag{3.16}$$

where the dimensionless variables are scaled as

$$\tau = \frac{tu_c}{l_c}; P = \frac{p}{\rho_2 u_c^2}$$

dimensionless shear stresses are given as

$$\tau_{rr} = 2\mu_m \left(\frac{\partial U}{\partial R}\right); \tau_{zz} = 2\mu_m \left(\frac{\partial V}{\partial Z}\right); \tau_{zr} = \tau_{rz} = \mu_m \left(\frac{\partial U}{\partial Z} + \frac{\partial V}{\partial R}\right)$$

$\mathbf{F}_{ST}$ and $\mathbf{F}_{ES}$ are dimensionless body forces due to interfacial tension and electric field respectively. Dimensionless numbers governing the system dynamic are Reynolds number, Weber Number and electric Bond number defined as

$$\mathrm{Re} = \frac{\rho_2 u_c l_c}{\mu_2}; We = \frac{\rho_2 {u_c}^2 l_c}{\gamma}; Bo_e = \frac{\epsilon_0 \epsilon_2 E_\infty^2}{\rho_2 {u_c}^2}$$

where γ is the coefficient of interfacial tension, ϵ_0 is the permittivity of vacuum and E_∞ is the electric field strength.

3.1.2.5 Governing Equations for Electric Field

Apart from hydrodynamics as the two phase system considered here is also coupled with a force induced by the applied electric field, an additional term for an electric body force ($\mathbf{F}_{ES}$) is included in Navier-Stokes equations. This dimensionless volumetric force can be calculated by taking the divergence of Maxwell stress tensor [29].

$$\mathbf{F}_{ES} = \nabla \cdot \left[\epsilon_m \left(\mathbf{EE} - \frac{1}{2}E^2\mathbf{I}\right)\right] = -\frac{1}{2}\mathbf{E}\cdot\mathbf{E}\nabla\epsilon_m + q_v\mathbf{E} + \nabla\left(\frac{1}{2}\mathbf{E}\cdot\mathbf{E}\frac{\partial\epsilon_m}{\partial\rho}\rho\right)$$

where q_v is the volume charge density, ϵ_m is the mean dimensionless electrical permittivity. Since we are considering both fluids as incompressible, the term of electrostrictive force due to change in density of the medium (third in RHS) is neglected. The first term in the RHS is the force due to polarization stresses and acts always in the direction normal to the interface. The second term is due to the interaction between the volumetric charge density and the electric field and acts always in the direction of electric field. Gauss law in terms of an electric displacement field can be given as

$$\nabla \cdot \mathbf{D} = q_v \tag{3.17}$$

The charge conservation law is simply an advection-diffusion equation given as

$$\frac{\partial q_v}{\partial \tau^e} + \nabla \cdot (U q_v) = -\nabla \cdot \mathbf{J} = \nabla \cdot (K_m \mathbf{E}) \tag{3.18}$$

The time scale for the charge dynamics $\tau_c^e = \epsilon_m/K_m$ is assumed to be very small as compared to the hydrodynamic time scale $\tau_c^v = \sqrt{\rho l_c^3/\gamma}$ where ρ and γ are mass density and interfacial tension of the fluid and l_c is the characteristic length scale. This is valid for a conductor-dielectric system or if both fluids are leaky dielectric in nature. If both fluids are perfectly dielectric, the condition is reversed i.e. hydrodynamic time scale becomes very small as compared to charge dynamics time scale.
So for a PD-PD system (both fluids as perfect dielectric), we assume that the bulk charge is zero i.e. $q_v = 0$ in equation (3.17), while in case of LD-LD system (both fluids as leaky dielectric), we assume the charge dynamics to be in quasi-steady state and set the substantial derivative for a charge variation with respect to time as zero in equation (3.18). Thus final simplified governing equations for electric field in these two cases come out to be

$$\nabla \cdot \mathbf{D} = \nabla \cdot (\epsilon_m \mathbf{E}) = 0 \text{ for PD-PD system}$$

$$\nabla \cdot \mathbf{J} = \nabla \cdot (K_m \mathbf{E}) = 0 \text{ for LD-LD system}$$

For both cases, these equations result in Laplace equation for an electric potential. However the dot product $\mathbf{D} \cdot \widehat{n}$ is continuous across the interface for a PD-PD system $\mathbf{J} \cdot \widehat{n}$ in case of LD-LD system. The mean dimensionless values of electrical conductivity and permittivity required for using these equations across the diffuse interface are smoothed using Heaviside function based weighted harmonic interpolation method [30] as follows

$$\frac{1}{\epsilon_m} = \frac{H_\epsilon(\phi)}{\alpha} + [1 - H_\epsilon(\phi)] = \frac{H_\epsilon(\phi) + \alpha\,[1 - H_\epsilon(\phi)]}{\alpha}$$

$$\frac{1}{K_m} = \frac{H_\epsilon(\phi)}{\beta} + [1 - H_\epsilon(\phi)] = \frac{H_\epsilon(\phi) + \beta\,[1 - H_\epsilon(\phi)]}{\beta}$$

where $\alpha = \epsilon_1/\epsilon_2$ and $\beta = K_1/K_2$.

As already stated earlier, electric force which is a surface force obtained by taking a divergence of Maxwell stress at the interface is converted into volumetric force and it is given for an incompressible system as

$$\mathbf{F}_{ES} = \begin{cases} -\frac{1}{2}\mathbf{E} \cdot \mathbf{E}\nabla\epsilon_m, & \text{for PD-PD system} \\ -\frac{1}{2}\mathbf{E} \cdot \mathbf{E}\nabla\epsilon_m + q_v\mathbf{E}, & \text{for LD-LD system} \end{cases} \tag{3.19}$$

The first term in the RHS originates due to polarization stresses acting in the direction of electric field; pointing from the medium with high permittivity to the one with low permittivity. The second term is the force on the volumetric charge due to electric field acting at the interface. However this representation does not satisfy the condition that

the volumetric force must become a surface force in the limit of $\epsilon \to 0$ (thickness of diffuse interface going to zero). To make it satisfy this condition, continuum surface force implementation method [30] is applied to get

$$\mathbf{F}_{ES} = \begin{cases} \frac{1}{2}\left((\mathbf{D}\cdot\widehat{n})^2\left(\frac{1}{\alpha}-1\right)-\left(\mathbf{E}\cdot\widehat{t}\right)^2(\alpha-1)\right)\widehat{n}\delta_\epsilon, \text{ for PD-PD system} \\ \frac{1}{2}\left((\mathbf{J}\cdot\widehat{n})^2\left(\frac{\alpha}{\beta^2}-1\right)-\left(E\cdot\widehat{t}\right)^2(\alpha-1)\right)\widehat{n}\delta_\epsilon, \text{ for LD-LD system} \\ +(\mathbf{J}\cdot\widehat{n})\left(\frac{\alpha}{\beta}-1\right)(\mathbf{E}\cdot\widehat{t})\,\widehat{t}\delta_\epsilon \end{cases} \tag{3.20}$$

where $\widehat{t}$ is tangential unit vector to the interface given as

$$\widehat{t} = \frac{\phi_Z}{\sqrt{\phi_R^2+\phi_Z^2}}\widehat{i} - \frac{\phi_R}{\sqrt{\phi_R^2+\phi_Z^2}}\widehat{j}$$

3.1.3 Numerical Methodology

The present work uses an in-house dual grid level set method based multi-fluid dynamics code in a 2D axisymmetric coordinate system – developed by Gada [19] and an additional electric field module developed by Lakdawala [31]. Gada and Sharma [19] proposed the dual grid level set method for 2D Cartesian coordinate system and hypothesised that finer grids are required for capturing the interface than flow properties in order to overcome the biggest drawback of using the level set method i.e. mass error. With the help of qualitative and quantitative results they showed that the dual grid level set method needs less computational time and achieves same accuracy as compared to the traditional level set method. Dual grid level set method uses finer grid for the equations which get coupled with momentum equations as a source term. Hence in this case, finer grid is used for calculating level set function and electric potential in order to accurately calculate interface normal, tangent and electric field vectors at the interface.

3.1.3.1 Dual grid Arrangement

Figures 3.11 and 3.12 show the arrangements of staggered grid and CV different variables in case of traditional level set method. We see that level set functions also have staggered grid points and are defined at the vertices of pressure CVs so that uniform stencils can be used while using higher order advection schemes such as Essentially Non-Oscillatory (ENO) and Weighted Essentially Non Oscillatory (WENO).
Whereas in case of dual grid level set method, figures 3.13 and 3.14 show staggered grid where level set functions and electric field variables are not only calculated at the vertices

of pressure CVs but also at velocity and pressure grid points. This grid is inherently doubly refined for level set function and electric field. It also useful for running higher order advection schemes since it is uniform everywhere.

3.1.3.2 Numerical Solution of Navier-Stokes and Level Set Equations

Semi-implicit pressure projection method under finite volume scheme is used solve Navier-Stokes equations on $m \times n$ grid. The continuity equation and diffusion term in the Navier-Stokes equation are treated implicitly, while volumetric forces and advection are treated explicitly. The advection and diffusion terms in the Navier-Stokes equation are discretised using 2nd order QUICK and central difference scheme, respectively.
The level set advection equation is solved explicitly on $2m \times 2n$ grid and is discretised using finite difference method with 3rd order Runge-Kutta and 5th order upwind WENO scheme for temporal and spacial terms respectively. The re-initialization equation is solved using 5th order WENO scheme.

3.1.3.3 Electric Field: Solution of Laplace Equation for Electric Potential

For both PD-PD and LD-LD systems, solution for electric potential is obtained by solving Laplace equation $\nabla^2\Theta = 0$. Finite volume method is used on a finer grid for its discretization. Conjugate gradient method is used for solving the resultant system of linear equations.
Figure 3.15 shows the geometrical parameters and grid points involved in the discretisation for a control volume for electric potential, represented by running index $2i$, $2j$. The diffusion coefficient which is an electrical property in this context is calculated at face centers of the control volume using volume weighted linear interpolation of its values at the neighbouring cell centers. Cell center values of electrical permittivity and conductivity across the interface are smoothened using the Heaviside function based weighted harmonic mean. It is important to notice that the thickness of diffuse interface for smoothening electrical properties $2\epsilon = 3\Delta R_\phi$ is half of that for smoothening flow properties $2\epsilon = 3\Delta R$ where ΔR_ϕ and ΔR are the elemental radial distance of the control volume for level set/electric potential and velocity/pressure respectively.

3.1.3.4 Calculation of Source Term for Electric Body Force

Values of electric field at all cell centers are calculated using those of electric potential and the relation $-\mathbf{E}_{2i,2j} = -(\nabla\Theta)_{2i,2j}$. Calculation is done using central difference scheme.

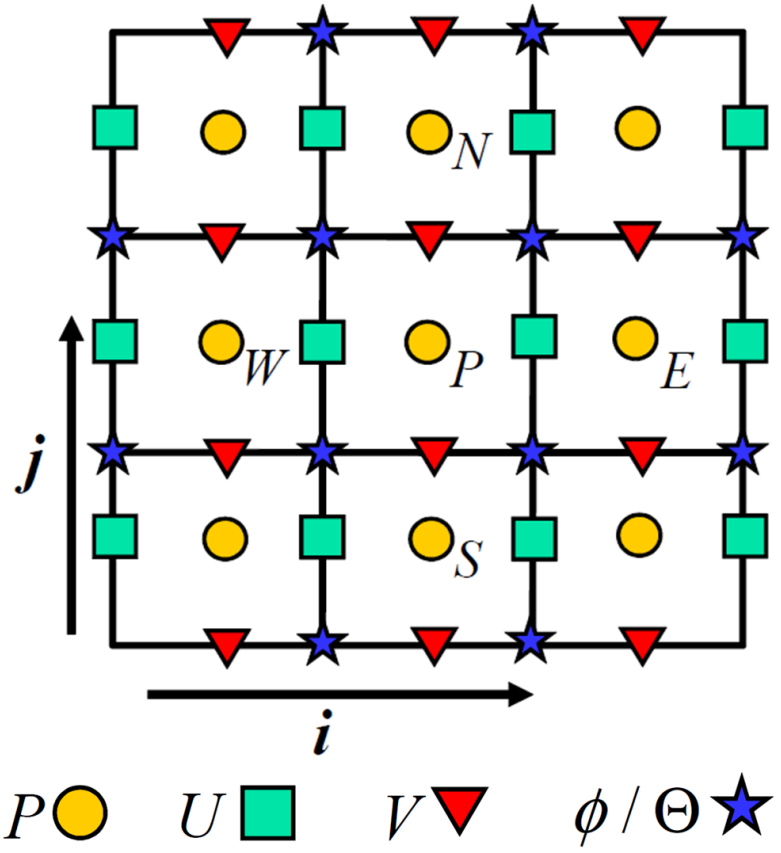

FIGURE 3.11: Staggered grid points of pressure, velocity, electric field variables/level set function for traditional level set method

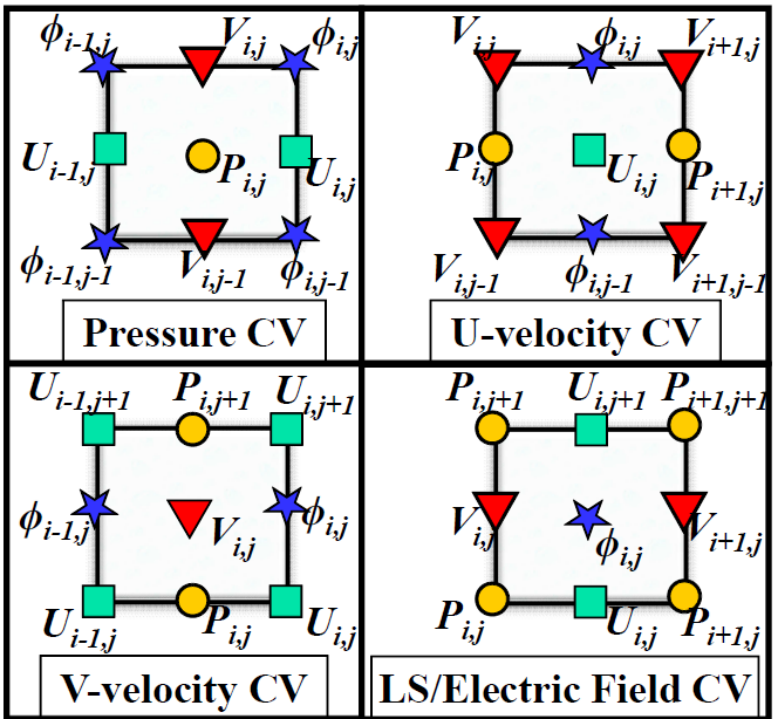

FIGURE 3.12: Staggered control volumes of pressure, velocity, electric field variables/level set function for traditional level set method

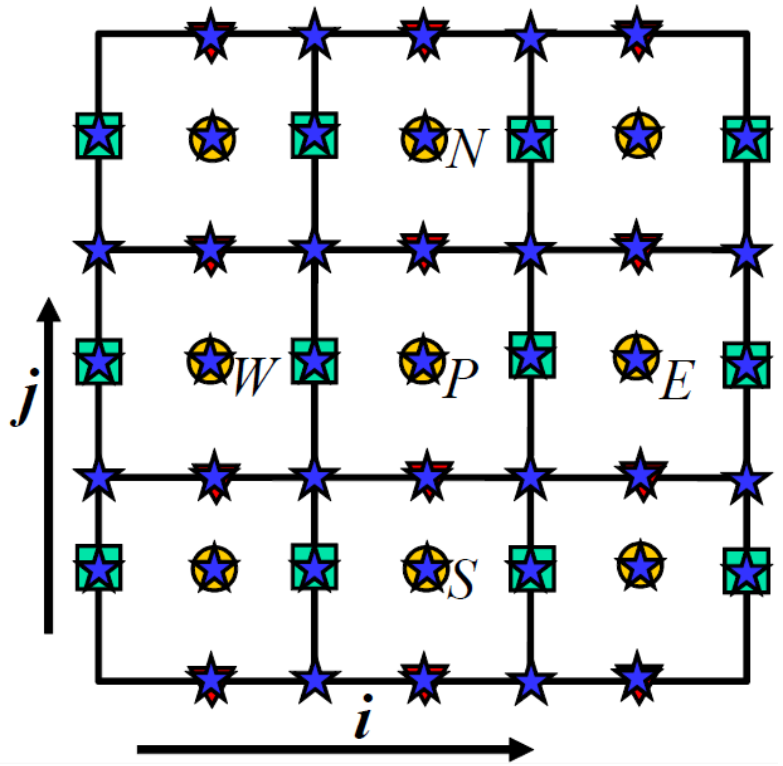

FIGURE 3.13: Staggered grid points of pressure, velocity, electric field variables/level set function for dual grid level set method

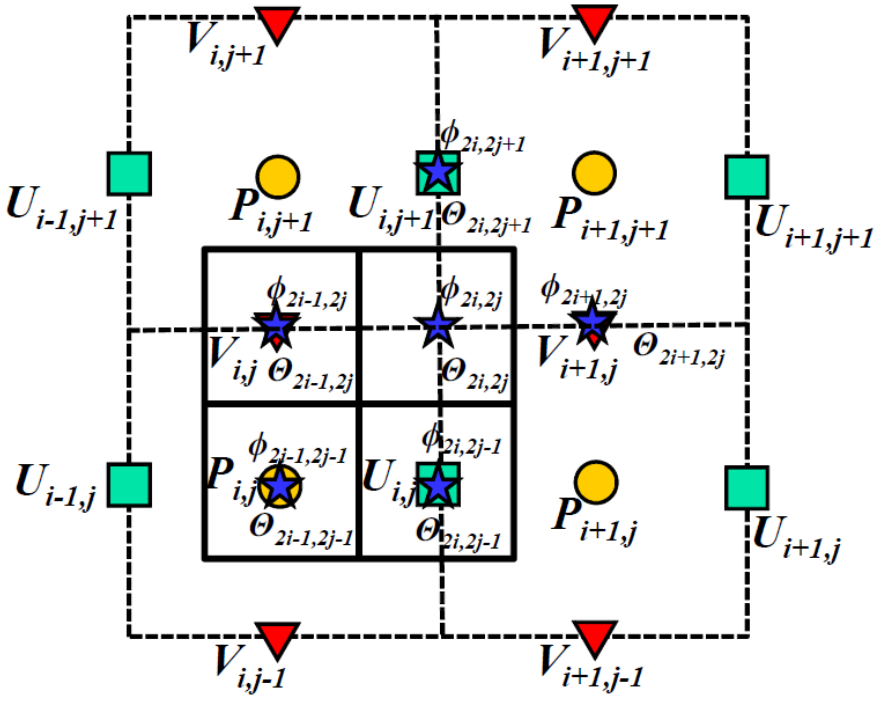

FIGURE 3.14: Staggered control volumes of pressure, velocity, electric field variables/level set function for dual grid level set method

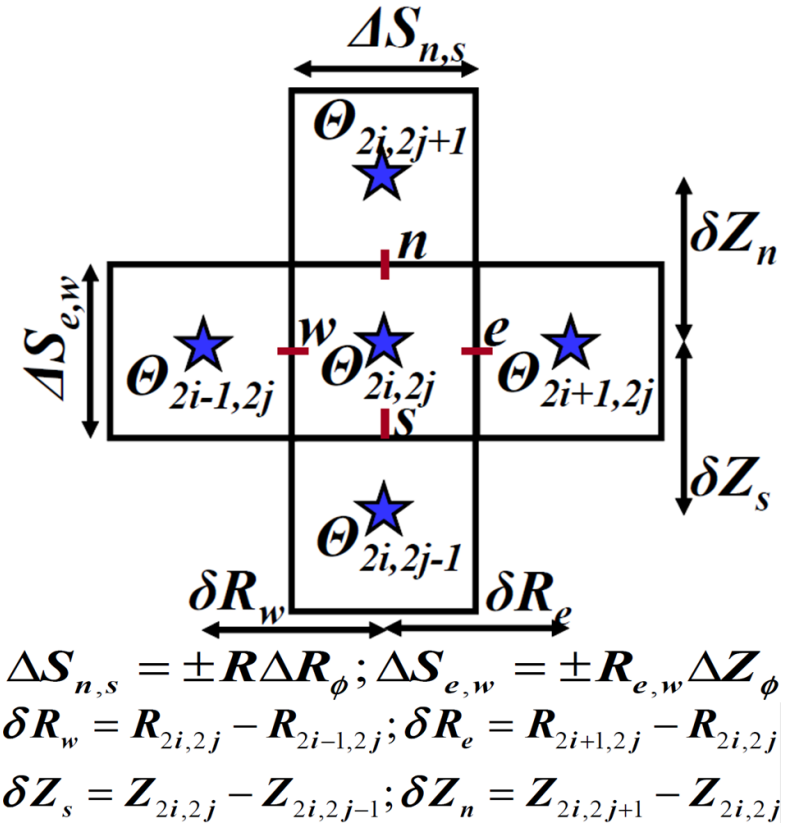

FIGURE 3.15: Geometric parameters and neighboring grid points involved in the discretization of electric field equations

After that electric displacement $\mathbf{D}_{2i,2j} = \epsilon_m \mathbf{E}_{2i,2j}$ and current density $\mathbf{J}_{2i,2j} = K_m \mathbf{E}_{2i,2j}$ are evaluated. In order to accurately capture the jump across the interface, electric field is calculated on a finer grid. Hence the curvature κ, normal and tangential unit vectors to the interface are also calculated on a finer grid.

3.1.3.5 Solution Algorithm

Following is the algorithm for electro-multi-fluid dynamic flow using dual grid level set method.

1. Initialize the LS field in the domain as per the initial interface configuration. Initialize velocities, pressure, voltage potential as zero.

2. Calculate the Heaviside function (equation (3.6)) and thermophysical, electrical property fields (equations (3.1), (3.2) and (3.20)) on finer grid.

3. Solve Laplace equation for voltage potential. Calculate electric field, electric displacement and electric current density in the domain. Extract functions ϕ, **E**, **D**, **J**

at pressure cell centers and calculate source terms (interfacial tension and electric body force) for Navier-Stokes equations.

4. Calculate n^{th} time-level advection and diffusion flux for Navier-Stokes equation. Predict the intermediate velocity field using pressure projection method.

5. Find the new time-level pressure field by solving pressure Poisson equation. Calculate the continuity-obeying velocity field by applying the velocity correction.

6. Determine the level set advecting velocity field at level set cell centers ($2m \times 2n$) by interpolating the velocity field ($m \times n$) obtained in the previous step.

7. Advect the level set field (equation (3.12)) and re-initialize level set function (equation (3.14)).

8. Return to step 2 until stopping criteria is met.

3.2 Results and Discussion

The code validation and performance study was performed by Lakdawala [32].

3.2.1 Parametric Details

Following entities have been used for non-dimensionalizing the set of governing equations: The radius of the nozzle R_1 as the length scale, the capillary velocity given as $u_c = \sqrt{\gamma/R_1\rho_1}$ as the characteristic velocity; and the potential difference between the nozzle and the grounded electrode Θ_0 as the characteristic potential scale. Following are the dimensionless parameters generated as a result of this arrangement which define the system:

1. Velocity of injection ($V_i = \overline{v_i}/u_c$) which quantifies the relative relevance of inertia of the jet as compared to capillary forces

2. The ratio of averaged inlet velocities of two fluids ($\theta = \overline{v_2}/\overline{v_1}$)

3. The ratio of densities ($\chi = \rho_2/\rho_1$) and viscosities ($\eta = \mu_2/\mu_1$) of fluids 1 and 2

4. The Reynolds number for inner fluid ($\text{Re} = \rho_1 u_c R_1/\mu_1$)

5. The ratio of electrical conductivities ($\alpha = \epsilon_1/\epsilon_2$) and permittivities ($\beta = K_1/K_2$) of fluids 1 and 2

6. The electric Bond number ($Bo_e = \epsilon_0\epsilon_2\Theta_0^2/\gamma R_1$) which is the ratio of electric stress and the capillary pressure

In this way, total parameters which characterize each case in the system are $V_i, \theta, \chi, \mu, \mathrm{Re}, \alpha, \beta, Bo_e$ The interface dynamics, jet behaviour and velocity profiles of both fluids are studied across wide ranges of three parameters namely the ratio of averaged inlet velocities of two fluids (θ), viscosity ratio (η) and the electric potential difference between the nozzle and the grounded electrode (Θ). Four values of $\theta = 0, 0.5, 2$ and 5 are considered. Viscosity ratio is varied as $0.2, 1$ and 3. Electric potential was changed by changing the electric bond number as $20, 22$ and 24.

3.2.2 Interface dynamics of Electrified Jet

As stated above, the interface dynamics is studied by changing electric potential, viscosity ratio and the initial average velocity ratio. Background liquid has been assumed to be lighter than the inner liquid in all cases that have been studied. Changing the electric potential corresponds to the change in the electric force on the multi fluid system. Since the inner liquid is considered dielectric with much higher electric conductivity and permittivity than outer liquid, the charge in the bulk of inner liquid quickly accumulates at the interface and consequently, electric force is concentrated at the interface only. Changing the viscosity ratio corresponds to changing the viscous stress at the interface. It also affects the radial momentum transport in both liquids and can eventually influence the interface dynamics. Changing the inlet average velocity ratio changes the inertial contribution in the flow of both liquids. It also changes the velocity gradient at the interface causing the change in the viscous stress which is one of the governing factors of interface dynamics.

3.2.3 Effect of Change in the Ratio of Average Inlet Velocities

Figure 3.16 shows how the interface topology changes by varying the average inlet velocity ratio. A common way to form a coflow with an inner jet for experimentalists is to increase the velocity of the outer liquid [33]. This results in an increase in the capillary number of the outer liquid $C_2 = \mu_2\overline{u_2}/\gamma$ where C_2 the velocity in the expression is the mean velocity for outer liquid. As seen from the expression, capillary number shows the relative effect of the viscous stress to the stress due to interfacial tension. Increasing the velocity of the outer fluid increases the inertial contribution to its flow thereby increasing its momentum flux. This increase affects the flow of inner liquid via the viscous stress at the interface in the direction of the coflow. Thus the inner fluid experiences the

interface stretching. As a result, its mode of flow can change from the dripping mode to the jet mode if the resultant inertial contribution is higher than the force due to interfacial tension. This can be quantified by Weber number $We_1 = \rho_1 \overline{u_1}^2 L/\gamma$ where L is the characteristic length scale comparable to the diameter of the jet and the velocity in the expression is the mean velocity of the inner liquid. Increase in the velocity of outer fluid can also initiate microdripping from the inner liquid jet if the viscous stress at the interface is high enough. So it has parallel effects as those due to increasing the electric field strength as it also acts on the inner liquid via Maxwell stress at the interface. Conversely, decreasing the velocity of the outer fluid decreases the momentum flux in it thereby exerting the viscous stress at the interface in the reverse direction and can be useful for going from jet to dripping mode.

Three cases are considered with following specifications:

$\chi = 0.5$; $\eta = 0.2$; $\alpha = 80$; $\beta = 1000$; $Bo_e = 30$ and $Re = 300$ with varying values of $\theta = 0$, 0.5 and 2.

It can be seen from the parameters α and β that outer liquid is assumed as a perfect dielectric and inner liquid as perfectly conducting. Density and viscosity ratios are taken such that outer liquid would be lighter and less viscous than inner liquid. The ratio of inlet average velocities has been varied as 0, 0.5 and 2. Outer liquid is stationary in the case of $\theta = 0$.

It can be observed from figure 3.16 that there is a dripping to jetting transition for all cases of velocity ratio. Firstly, a thin jet with a low breakup length and is formed which can be seen in the parts a(2)-a(4), b(2)-b(4) and c(2)-c(5). The flow mode transition occurs to tip streaming with time in all cases. This can be attributed to the effect of viscous stress at the interface by the outer liquid. In case of $\theta = 0$, the jet elongates earlier than other cases since the viscous stress at its interface is lower and is not enough for dripping to continue. In the dripping regime in all cases, viscous drag and the interfacial tension stress are the two competing forces which are experienced at the interface of the growing droplet. Interfacial tension stress holds the droplet at the tip while viscous drag pulls it downstream. At first the droplet is dominated by the interfacial tension force but viscous drag increases afterwards and becomes comparable to interfacial tension stress. Initial domination of interfacial tension stress causes dripping and balancing it by the viscous stress causes the jet to stabilize. In case of $\theta = 2$, dripping continues longer till c(6). It is again the viscous drag from the outer liquid which drives the drop formation. The dripping to jetting transition occurs at a(5) for the case of $\theta = 0$, at b(6) for $\theta = 0.5$ and at c(7) for $\theta = 2$ once the jet stabilizes. All jets are eventually stabilized confirming the complete transition to the jet mode and the gradient of net stress at the interface relaxes.

Figure 3.17 shows the displacement of the tip of inner liquid jet as a function of time for all three cases. At many instances within a plot we see a retracting of a jet by significant

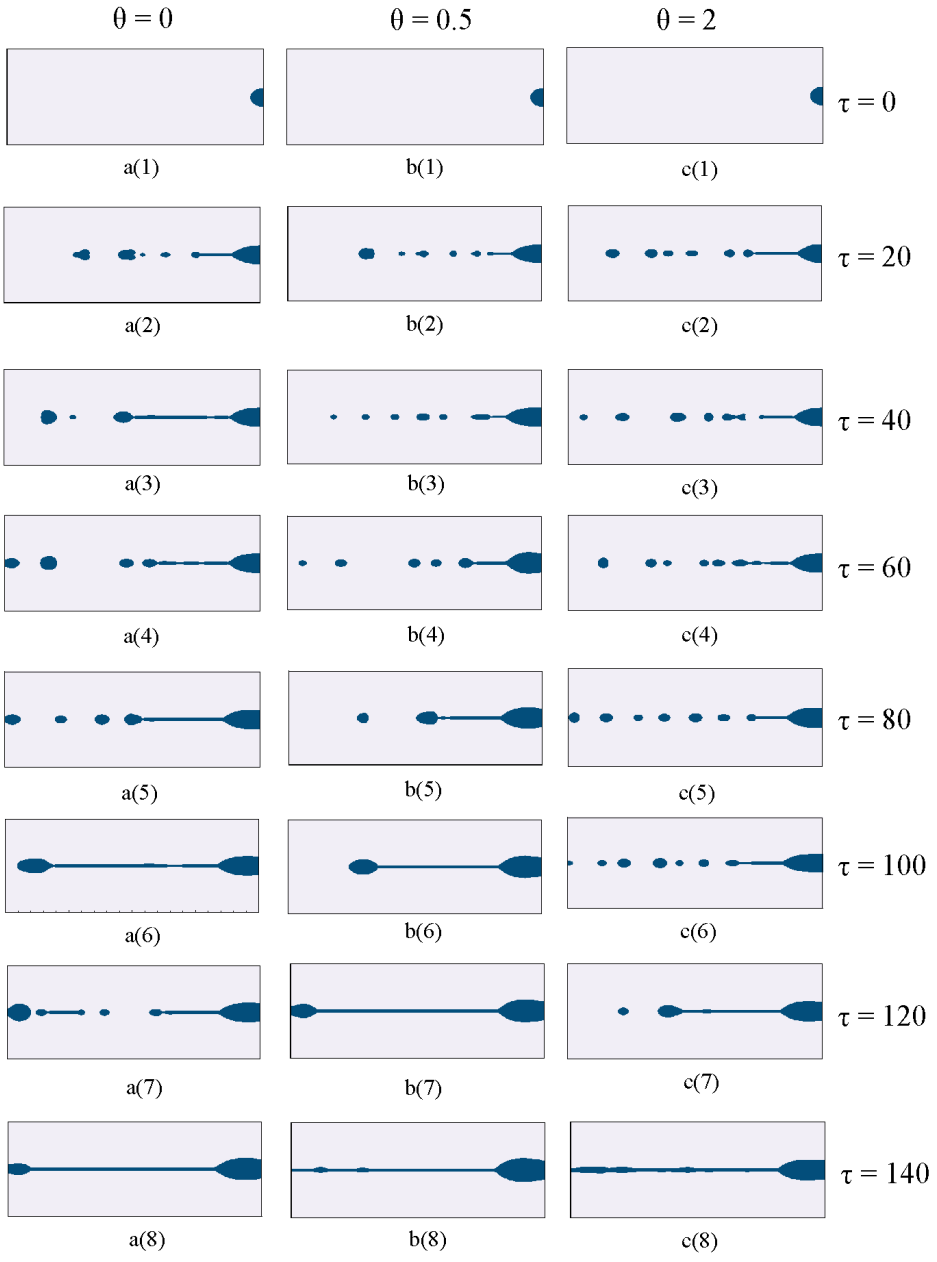

FIGURE 3.16: EHD jet evolution for different values of the ratio of average inlet velocities (a) $\theta = 0$ (b) $\theta = 0.5$ (c) $\theta = 2$

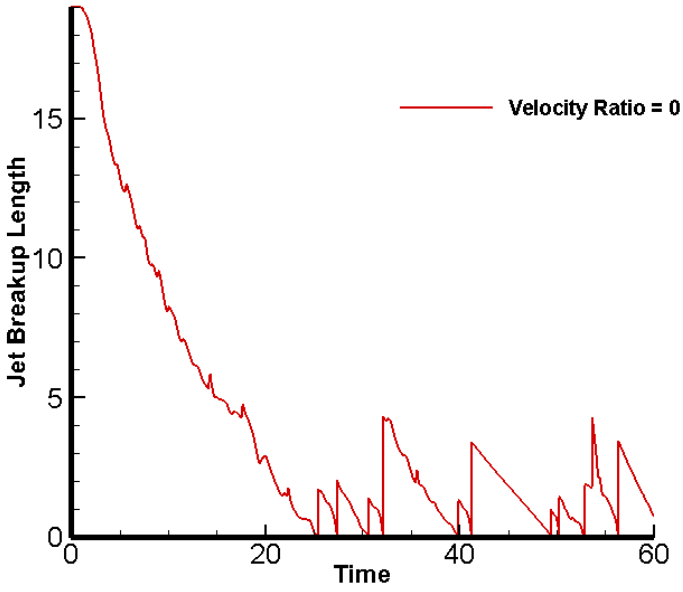
Velocity Ratio = 0
Jet Breakup Length
Time
0
5
10
15
0
20
40
60

(a)

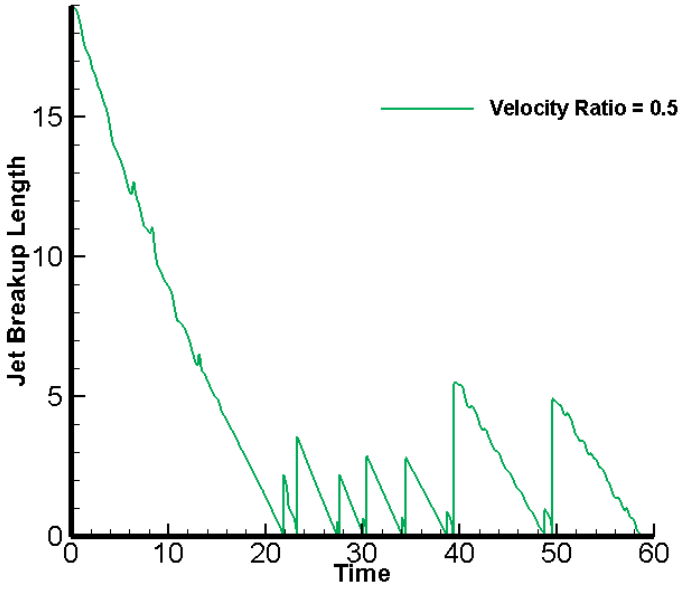
Velocity Ratio = 0.5
Jet Breakup Length
Time
0
5
10
15
0
10
20
30
40
50
60

(b)

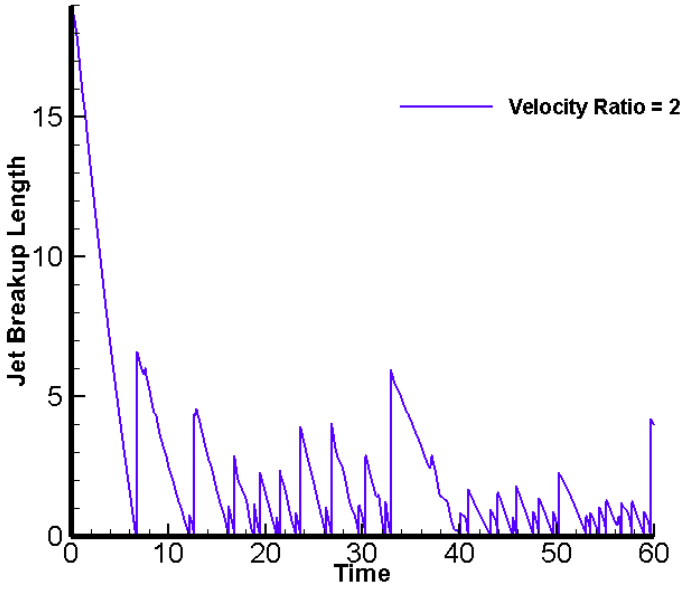

(c)

FIGURE 3.17: Variation in the position of the tip of EHD jet with time at different values of inlet average velocity ratio (a) $\theta = 0$ (b) $\theta = 0.5$ (c) $\theta = 2$

magnitude. The position after retracting corresponds to the one after the detachment of a primary droplet from the jet. Small fluctuations in the position are due to fast changing topology of the interface while evolving.

All slanted curves in all figures represent the forward marching of the tip of the inner liquid jet. The zigzag nature of each curve is due to the growth of the jet followed by the detachment of the primary droplet at its tip. Observing all slanted curves in all cases, we see that the slope of a curve in case of $\theta = 2$ (figure (c)) is steeper than that in case of $\theta = 0.5$ (figure (b)) which is steeper than that in the case of $\theta = 0$ (figure (a)). This shows that the increase in the velocity of the outer liquid accelerates the inner liquid jet. Also, the height to which the tip retracts just after the breakup of a primary droplet from the jet gives us a qualitative idea about the volume of the detached droplet. If we compare these heights between these cases, we see that the average size of the detached droplet goes on decreasing as we go from $\theta = 0$ to 2. This shows that the droplet size decreases with increasing the outer liquid velocity. Furthermore, observing the number of zigzag curves tells us about the number of droplets detached from the jet. We see that the number of droplets formed in case of $\theta = 2$ is significantly higher than other cases. This indicates that increasing the outer liquid velocity enhances the microdripping of inner liquid jet.

3.2.4 Effect of Change in Electric Potential

Figure 3.18 shows the interface evolution with increasing the electric potential which can be done by changing the electric Bond number. Since the spacing between the nozzle and the opposite grounded electrode is constant, increasing the nozzle potential also increases the electric field strength across the whole domain thereby increasing the magnitude of Maxwell stress at the interface.
Three cases are considered with following specifications
$\chi = 0.5$; $\eta = 1.5$; $\theta = 2.0$; $\alpha = 80$; $\beta = 1000$; $Re = 200$ with varying values of $Bo_e = 0$, 20 and 30.
Specified parameters show that the system considered has outer liquid which lighter, more viscous and has twice the inlet average velocity as that of inner liquid.
It can be clearly seen from figure 3.18 that the flow mode of inner liquid changes from dripping to microdripping and eventually to jet mode. Figures a(1)-a(5) correspond to the dripping mode which is characterized as the case when the droplets formed have uniform size and the frequency of their formation or ejection from the nozzle is regular. Also the dynamics of a(1)-a(5) is quite slow if compared with other two cases, which shows that the applied electric field or the increase in the electric potential enhances the axial mass transfer of the inner liquid. In transition from b(1) to b(2) or c(1) to c(2), we see that cone shaped meniscus is formed at the tip of the nozzle from which a continuous jet of inner liquid emanates. This geometric formation is called a Taylor cone and it corresponds to the minimum energy surface as a result of the balance between the interfacial tension stress and Maxwell stress at the nozzle tip. In case of the outer fluid flowing, interfacial tension balances Maxwell stress and the change in the viscous stress due to the changed interfacial velocity. Accordingly the geometric specifications of the cone i.e. cone angle, diameter etc. change. In the dynamics of a(1)-a(5), inner liquid emanates from the capillary as discreet droplets due to the interfacial tension stress dominating the viscous stress at the interface from the outer liquid. In the case of an electric potential exerted externally, since the inner liquid is not perfectly dielectric, the charges induced migrate quickly at the interface. The time scale of this migration is assumed to be very small as compared to the hydrodynamic time scale (See section 2.6 for more details.). So it can be assumed that as soon as the electric field is switched on the charges come to the interface instantaneously. This creates a net charge distribution at the interface which interacts with the applied electric field setting the interfacial charge in motion and causing the interfacial force called Maxwell stress. There is an interesting concept defined in the literature called the *effective electromechanical surface tension* of the droplet-liquid interface, which gets lowered on applying the electric field. This decreases the size of droplets that break off the capillary and it clearly seen on comparing a(3)-a(5) to b(3)-b(5). It can also be seen from these pictures that the frequency of

droplet emanation increases drastically on introducing or increasing the electric field. When the field strength crosses a critical value, the mode of droplet emission changes from dripping to jetting. This is observed on comparing a(4), b(4), c(4) or a(5), b(5) and c(5). This thread like profile is also called microdripping mode. In this mode of flow, the radius of primary droplet emanated is of the order of magnitude less than the capillary radius. The sizes of these droplets formed are also non-uniform as can be seen from b(3), c(3), b(4) and c(4). However it is difficult to attain microdripping mode in practice. One reason is that a different mode of droplet formation might coexist with microdripping for the same range of voltages or electric Bond numbers. Another reason is that the required strengths of electric field in order to attain microdripping mode may be so large that it may cause dielectric breakdown of the liquid domain. The interface dynamics of the jet and droplets is characterized by the balance of several forces at the interface in which electric and viscous forces act against interfacial tension force and inertial force of inner liquid. Hence changing the interfacial viscous stress by manipulating the velocity of outer fluid should be helpful in attaining the microdripping mode with moderate strengths of electric field.

It can be observed from b(4), b(5) and c(4), c(5) that the tip of the conical meniscus is displaced away from the capillary. This is an initiating step for another mode of flow of inner liquid called micro-jet. In such scenarios, electric field strength increases so that Maxwell stress and viscous stress at the interface overcome the interfacial tension stress causing a micro-jet to be issued from the cone meniscus. As opposed to microdripping mode, micro-jet mode has the tip of the cone few orders of magnitude downstream from the nozzle inlet.

Results depicted in figure 3.18 can be summarised as follows. Firstly, taking the fall in the effective electromechanical surface tension of the interface with the increase in the electric field strength into consideration, it is intuitive that the size of primary droplet decreases and the dripping rate increases. Moreover, decrease in the effective electromechanical surface tension allows the jet breakup length to increase.

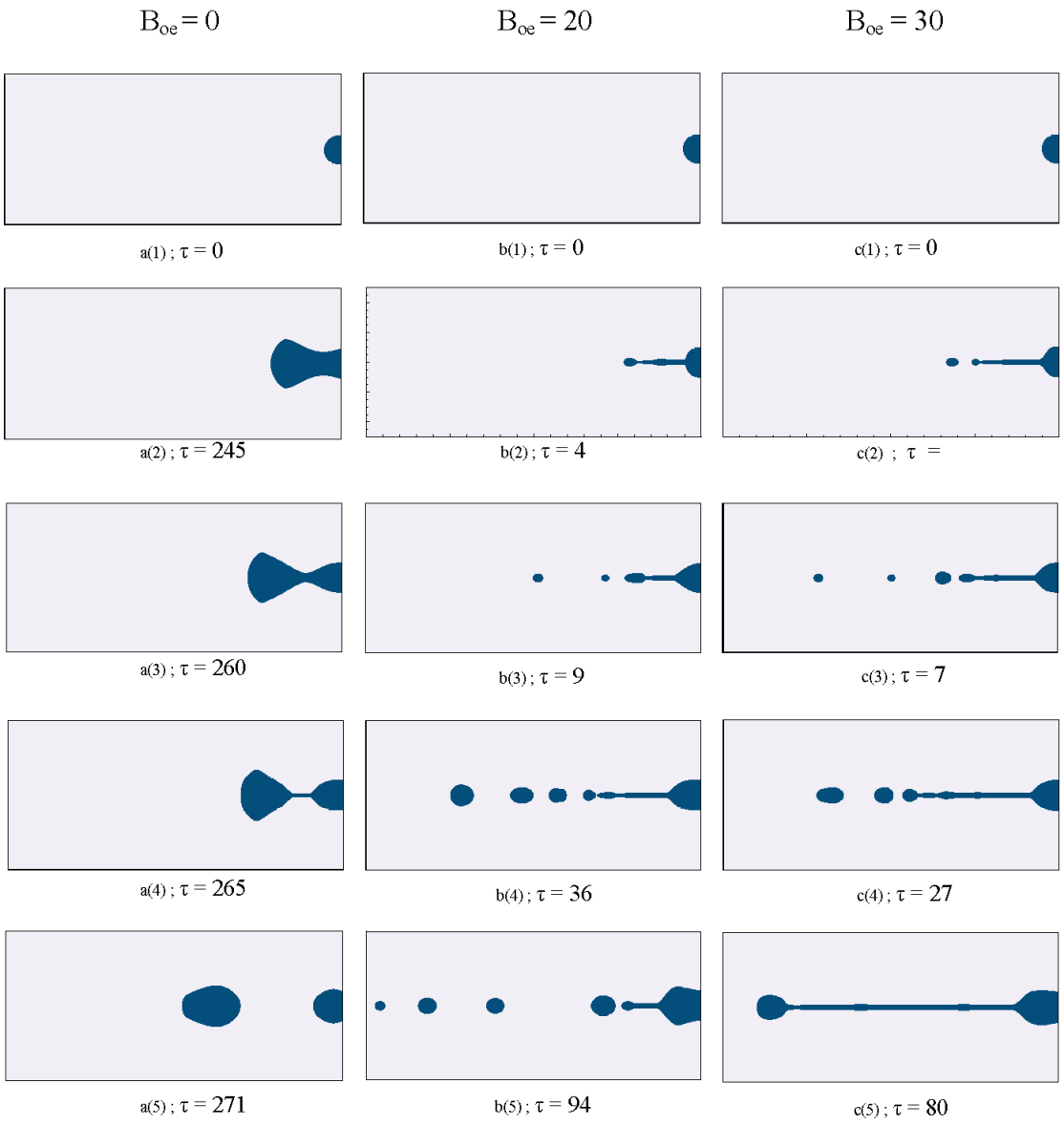

FIGURE 3.18: EHD jet evolution for different values of electric Bond number

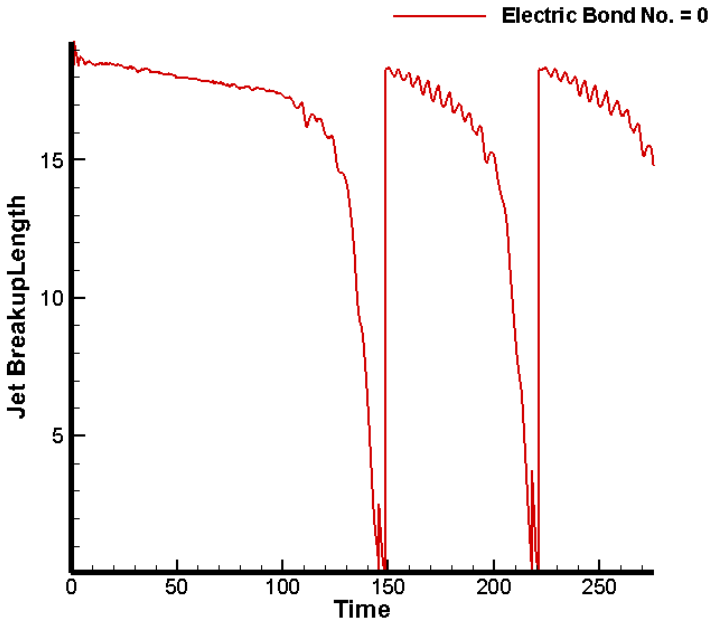

(a)

From figure 3.19, it can be observed that the droplet formation is regular in case of zero electric field (figure (a)) and gets irregular once electric field is introduced. Also the volume of droplets formed in case of zero electric field is very large as compared to other two cases, which implies that the electric field reduces the effective electromechanical tension at the interface causing microdripping before the eventual development of the jet. There is a very slight increase in the slope of slanted curves on comparing figures (b) and (c), which indicates that increasing the outer fluid velocity has a greater impact on accelerating the inner liquid jet than increasing the electric field.

3.2.5 Effect of Change in the Viscosity Ratio

Figure 3.20 shows the effect of changing the viscosity ratio on the inner fluid jet. Viscosities of individual liquids can also be changed by changing their capillary number which quantifies the relative magnitude of viscous force at the interface to the force due to interfacial tension. Increase in the viscosity increases the capillary number and this causes significant increase in the thread length of the jet of inner fluid because of the enhancement of the damping of disturbances on the surface of the thread that is provided by increase in the relative importance of the viscous force at the interface. Lister and Stone performed a stability analysis of the capillary jet of a viscous thread surrounded by another viscous liquid and they found that no matter how small the viscosity of outer background liquid is, as the breakup singularity is approached the viscous shear stresses

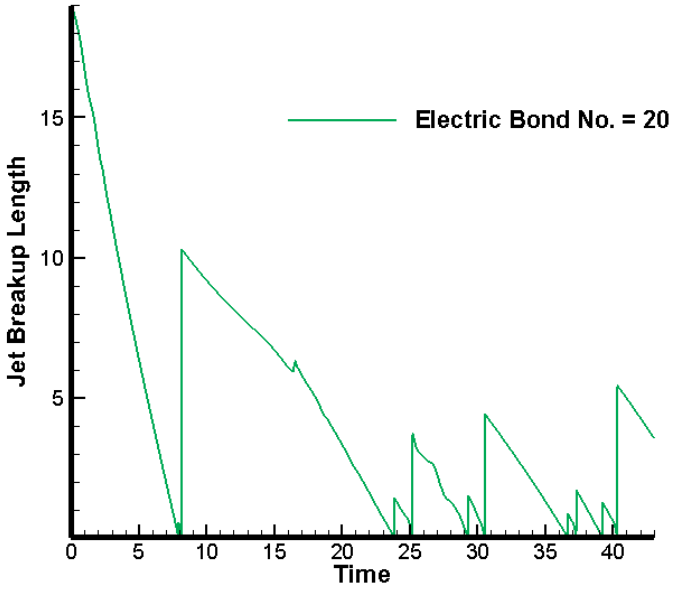

(b)

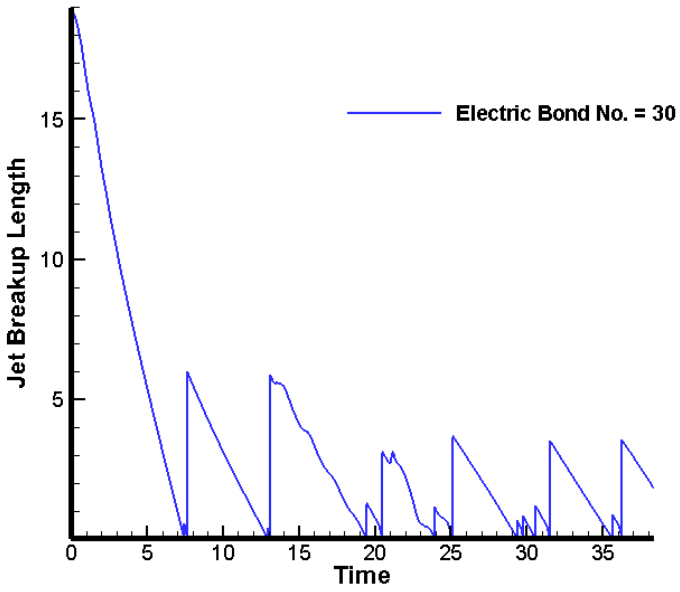

(c)

FIGURE 3.19: Variation in the position of the tip of EHD jet with time at different values of electric Bond number (a) $Bo_e = 0$ (b) $Bo_e = 20$ (c) $Bo_e = 30$

exerted by outer liquid and associated with the axial motion of the thread become comparable to the viscous stresses in the bulk of inner liquid which are associated with the thread extension. The external viscous stresses act as a brake and slow the growth of the instability down. As opposed to viscous forces, interfacial tension force not only moves the fluid particles of the jet, but also pushes the outer liquid away to allow the instability to grow. Tomotika [34] did a stability analysis of a cylindrical thread of viscous liquid surrounded by another viscous liquid. This analysis shows that the stability effect to the jet breakup process is provided by viscosities of both inner and outer liquids.
Two cases are considered with following specifications:
$\chi = 0.5$; $\theta = 2.0$; $\alpha = 80$; $\beta = 1000$; $Bo_e = 28$ and $Re = 200$ with varying values of $\eta = 0.2$ and 1.
One of the two cases has inner liquid five times viscous than outer liquid while other cases takes inner viscosity to be equal to outer viscosity. Outer liquid has twice the average inlet velocity than the inner one.
Figures a(1)-a(5) show that the dripping flow mode of inner liquid continues for a longer time in case of $\eta = 0.2$ as compared to that with the case $\eta = 1$. This is consistent with the conclusions from the literature. The viscous stress at the interface which is one of the responsible factors for the stability of the electrohydrodynamic jet has a lower magnitude in the case of $\eta = 0.2$ as compared to that in the case of $\eta = 1$. Hence relative contribution of the stress due to interfacial tension on the jet dynamics is higher in case of $\eta = 0.2$, which causes the instabilities more. Growth of instability helps in the growth of undulation of the interface which eventually causes the droplets to emanate. Whereas it can be seen from figures b(1)-b(5) that the development of the jet mode in case of $\eta = 1$ is much faster due to relatively higher contribution of interfacial viscous stress.

3.3 Conclusion

In this work, physical description in the dripping and microdripping flow mode of an electrostatically driven meniscus having a hydrodynamic interaction with a coflowing liquid in background is presented with the help of dual grid level set method.
According to the results, the mode of breakup of an electrified jet changes from dripping to microdripping mode as the electrostatic contribution to the net force at the interface overcomes the contribution by interfacial tension which is in qualitative agreement with the previous experiments by Cloupeau and Prunet-Foch [8], Zhang and Basaran [7]. It has been found that increasing the viscosity ratio increases the jet stability. Instability introduced during the jet flow dies down as a result of increased viscous

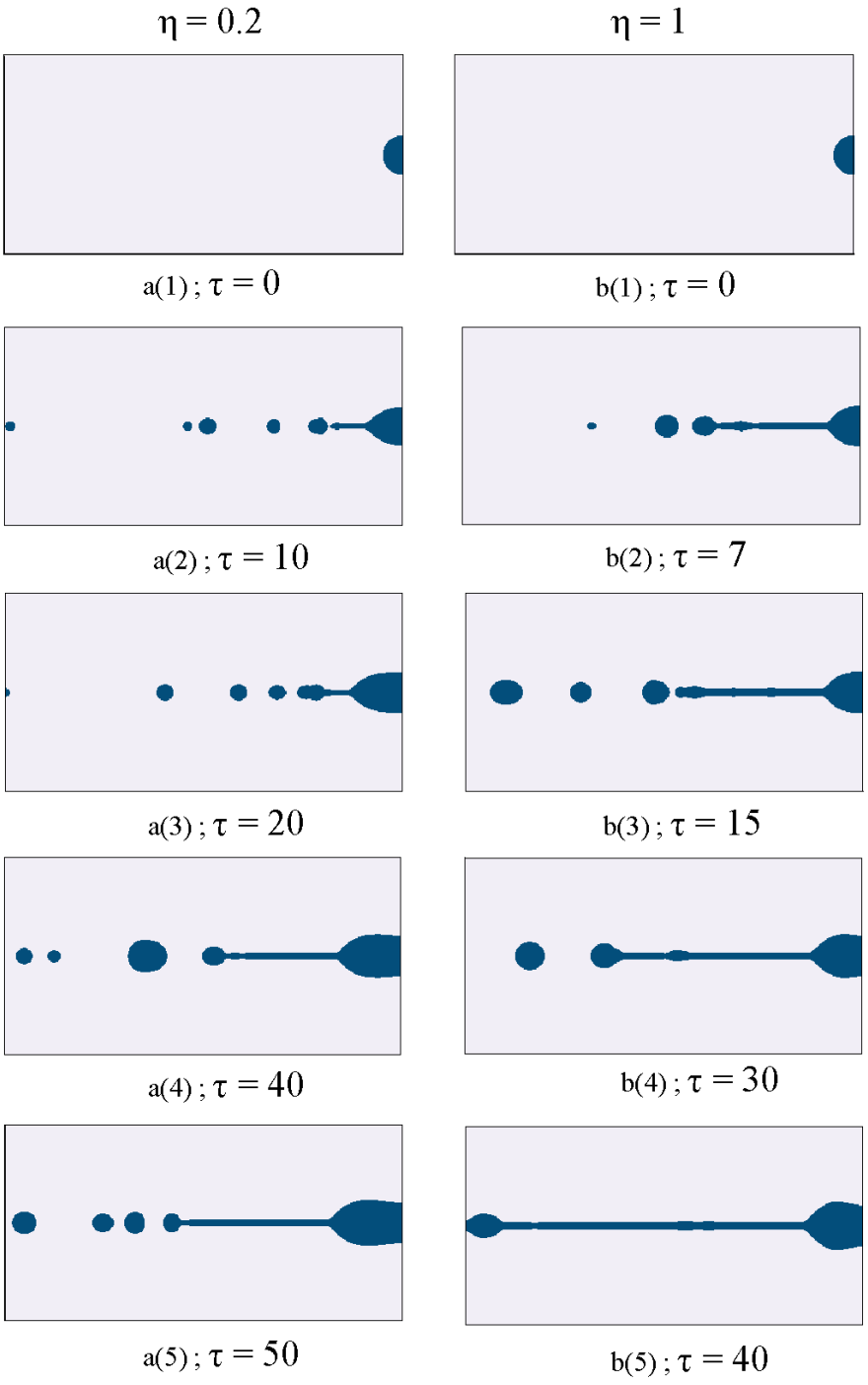

FIGURE 3.20: EHD jet evolution for different values of viscosity ratio

forces at the interface due to increased viscosity of outer liquid. Increasing the inertia of the outer liquid accelerates the inner liquid jet however at the same time decreases its breakup time. Also the droplet size decreases and the number of droplets formed increases. Thus increasing the inertia of outer liquid causes a transition from jet mode to microdripping mode. In addition to external electric field, introducing the flow of the outer fluid can be viewed as an addition tool towards manipulating the balance between the governing forces and thus adjusting the flow of inner liquid to a desired mode for different applications.

Bibliography

[1] John Zeleny. The electrical discharge from liquid points, and a hydrostatic method of measuring the electric intensity at their surfaces. *Physical Review*, 3(2):69, 1914.

[2] John Zeleny. On the condition of instability of electrified drops, etc. In *Proc. Camb. Phil. Soc*, volume 18, pages 71–83, 1915.

[3] John Zeleny. Instability of electrified liquid surfaces. *Physical Review*, 10(1):1, 1917.

[4] Geoffrey Taylor. Disintegration of water drops in an electric field. In *Proceedings of the Royal Society of London A: Mathematical, Physical and Engineering Sciences*, volume 280, pages 383–397. The Royal Society, 1964.

[5] Toru Takamatsu, Yoshiki Hashimoto, Manabu Yamaguchi, and Takashi Katayama. Theoretical and experimental studies of charged drop formation in a uniform electric field. *Journal of Chemical Engineering of Japan*, 14(3):178–182, 1981. doi: 10.1252/jcej.14.178.

[6] Toru Takamatsu, Yoshiki Hashimoto, Manabu Yamaguchi, and Takashi Katayama. Formation of single charged drops in a non-uniform electric field. *Journal of Chemical Engineering of Japan*, 16(4):267–272, 1983. ISSN 0021-9592.

[7] Xiaoguang Zhang and Osman a. Basaran. Dynamics of drop formation from a capillary in the presence of an electric field. *Journal of Fluid Mechanics*, 326(-1): 239, 1996. ISSN 0022-1120. doi: 10.1017/S0022112096008300.

[8] M. Cloupeau and B. Prunet-Foch. Electrostatic spraying of liquids in cone-jet mode. *Journal of Electrostatics*, 22(2):135–159, 1989. ISSN 03043886. doi: 10.1016/0304-3886(89)90081-8.

[9] J. Fernández De La Mora and I. G. Loscertales. The current emitted by highly conducting Taylor cones. *Journal of Fluid Mechanics*, 260(-1):155, 1994. ISSN 0022-1120. doi: 10.1017/S0022112094003472.

[10] J Rosell-Llompart and J Fernández De La Mora. Generation of monodisperse droplets 0.3 to 4 μm in diameter from electrified cone-jets of highly conducting and viscous liquids. *Journal of Aerosol Science*, 25(6):1093–1119, 1994.

[11] V. R. Gundabala, N. Vilanova, and a. Fernández-Nieves. Current-Voltage characteristic of electrospray processes in microfluidics. *Physical Review Letters*, 105(15): 1–4, 2010. ISSN 00319007. doi: 10.1103/PhysRevLett.105.154503.

[12] a. M. Gañán Calvo, J. Dávila, and a. Barrero. Current and droplet size in the electrospraying of liquids. Scaling laws. *Journal of Aerosol Science*, 28(2):249–275, 1997. ISSN 00218502. doi: 10.1016/S0021-8502(96)00433-8.

[13] RPA Hartman, J-P Borra, DJ Brunner, JCM Marijnissen, and B Scarlett. The evolution of electrohydrodynamic sprays produced in the cone-jet mode, a physical model. *Journal of electrostatics*, 47(3):143–170, 1999.

[14] Robert Petrus Adrianus Hartman, DJ Brunner, DMA Camelot, JCM Marijnissen, and B Scarlett. Electrohydrodynamic atomization in the cone–jet mode physical modeling of the liquid cone and jet. *Journal of Aerosol science*, 30(7):823–849, 1999.

[15] F. J. Higuera. Numerical computation of the domain of operation of an electrospray of a very viscous liquid. *Journal of Fluid Mechanics*, 648:35, 2010. ISSN 0022-1120. doi: 10.1017/S0022112009993235.

[16] P. K. Notz and O. A., Basaran. Dynamics of drop formation in an electric field. *Journal of colloid and interface science*, (1):218–237. ISSN 1095-7103. doi: 10.1006/jcis.1999.6136.

[17] Liang Kuang Lim, Jinsong Hua, Chi-Hwa Wang, and Kenneth A Smith. Numerical simulation of cone-jet formation in electrohydrodynamic atomization. *AIChE journal*, 57(1):57–78, 2011.

[18] MA Herrada, JM López-Herrera, AM Gañán-Calvo, EJ Vega, JM Montanero, and S Popinet. Numerical simulation of electrospray in the cone-jet mode. *Physical Review E*, 86(2):026305, 2012.

[19] Vinesh H. Gada and Atul Sharma. On a Novel Dual-Grid Level-Set Method for Two-Phase Flow Simulation. *Numerical Heat Transfer, Part B: Fundamentals*, 59 (1):26–57, 2011. ISSN 1040-7790. doi: 10.1080/10407790.2011.540956.

[20] David Jeffrey Griffiths and Reed College. *Introduction to electrodynamics*, volume 3. prentice Hall Upper Saddle River, NJ, 1999.

[21] Stanley Osher and James A Sethian. Fronts propagating with curvature-dependent speed: algorithms based on hamilton-jacobi formulations. *Journal of computational physics*, 79(1):12–49, 1988.

[22] Mark Sussman, Peter Smereka, and Stanley Osher. A Level Set Approach for Computing Solutions to Incompressible Two-Phase Flow. ISSN 00219991.

[23] Y.-C. Chang, T Hou, B Merriman, and S Osher. Eulerian Capturing Methods Based on a Level Set Formulation for Incompressible Fluid Interfaces. *J. Comput. Phys.*, 124(124):449–464, 1996. ISSN 00219991. doi: 10.1006/jcph.1996.0072.

[24] Gihun Son. a Level Set Method for Incompressible Two-Fluid Flows With Immersed Solid Boundaries. *Numerical Heat Transfer, Part B: Fundamentals*, 47(5):473–489, 2005. ISSN 1040-7790. doi: 10.1080/10407790590919252.

[25] Gihun Son and Nahmkeon Hur. A Level Set Formulation for Incompressible Two-Phase Flows on Nonorthogonal Grids. *Numerical Heat Transfer, Part B: Fundamentals*, 48(3):303–316, 2005. ISSN 1040-7790. doi: 10.1080/10407790590959762.

[26] Youngho Suh and Gihun Son. A Level-Set Method for Simulation of a Thermal Inkjet Process. *Numerical Heat Transfer, Part B: Fundamentals*, 54(2):138–156, 2008. ISSN 1040-7790. doi: 10.1080/10407790802182661.

[27] Vinesh H. Gada and Atul Sharma. On Derivation and Physical Interpretation of Level Set Method–Based Equations for Two-Phase Flow Simulations. *Numerical Heat Transfer, Part B: Fundamentals*, 56(4):307–322, 2009. ISSN 1040-7790. doi: 10.1080/10407790903388258.

[28] J. U. Brackbill. A continuum method for modeling surface tension. *Journal of Computational Physics*, 100(2):335–354, 1992. ISSN 00219991. doi: 10.1016/0021-9991(92)90240-Y.

[29] Lev Davidovich Landau, JS Bell, MJ Kearsley, LP Pitaevskii, EM Lifshitz, and JB Sykes. *Electrodynamics of continuous media*, volume 8. elsevier, 1984.

[30] Gaurav Tomar, Daniel Gerlach, Gautam Biswas, Norbert Alleborn, Ashutosh Sharma, Franz Durst, Samuel WJ Welch, and Antonio Delgado. Two-phase electrohydrodynamic simulations using a volume-of-fluid approach. *Journal of Computational Physics*, 227(2):1267–1285, 2007.

[31] Absar Lakdawala, Vinesh H. Gada, and Atul Sharma. On Dual-Grid Level-Set Method for Computational-Electro-Multifluid-Dynamics Simulation. *Numerical Heat Transfer, Part B: Fundamentals*, (2):161–185, . ISSN 1040-7790. doi: 10.1080/10407790.2014.949582.

[32] Absar Lakdawala. *A Novel Level-Set based CMFD Methodology and its Application to Interface Dynamics of Jet Breakup with and without Electric Field.* PhD thesis, Indian Institute of Technology Bombay, 2015.

[33] Andrew S. Utada, Alberto Fernandez-Nieves, Howard a. Stone, and David a. Weitz. Dripping to jetting transitions in coflowing liquid streams. *Physical Review Letters*, 99(9):1–4, 2007. ISSN 00319007. doi: 10.1103/PhysRevLett.99.094502.

[34] S Tomotika. On the instability of a cylindrical thread of a viscous liquid surrounded by another viscous fluid. In *Proc. Roy. Soc. A*, volume 150, pages 322–337, 1935.

[35] Robert T. Collins, Michael T. Harris, and Osman a. Basaran. Breakup of electrified jets. *Journal of Fluid Mechanics*, 588(August 2015), 2007. ISSN 0022-1120. doi: 10.1017/S0022112007007409.

[36] Jens Eggers and Emmanuel Villermaux. Physics of liquid jets. *Reports on Progress in Physics*, 71(3):036601, 2008. ISSN 0034-4885. doi: 10.1088/0034-4885/71/3/036601.

[37] C H Chen. Electrohydrodynamic Stability Chuan-Hua.

[38] Robert T. Collins, Jeremy J. Jones, Michael T. Harris, and Osman a. Basaran. Electrohydrodynamic tip streaming and emission of charged drops from liquid cones. *Nature Physics*, 4(2):149–154, 2008. ISSN 1745-2473. doi: 10.1038/nphys807.

[39] John R. Lister and Howard a. Stone. Capillary breakup of a viscous thread surrounded by another viscous fluid. *Physics of Fluids*, (11):2758. ISSN 10706631. doi: 10.1063/1.869799.

[40] Stanley Osher. an Improved Level Set Method for Incompressible Two-Phase Flows. *Computers & Fluids*, 27(97):663–680, 1998.

[41] J. D. Sherwood. Breakup of fluid droplets in electric and magnetic fields. *Journal of Fluid Mechanics*, 188(-1):133, 1988. ISSN 0022-1120. doi: 10.1017/S0022112088000667.

[42] Damir Juric and Grétar Tryggvason. Computations of boiling flows. *International Journal of Multiphase Flow*, 24(3):387–410, 1998. ISSN 03019322. doi: 10.1016/S0301-9322(97)00050-5.

[43] Absar M. Lakdawala, Vinesh H. Gada, and Atul Sharma. A dual grid level set method based study of interface-dynamics for a liquid jet injected upwards into another liquid. *International Journal of Multiphase Flow*, pages 206–220, . ISSN 03019322. doi: 10.1016/j.ijmultiphaseflow.2013.11.009.

[44] Andrew S. Utada, Alberto Fernandez-Nieves, Jose M. Gordillo, and David a. Weitz. Absolute instability of a liquid jet in a coflowing stream. *Physical Review Letters*, 100(1), 2008. ISSN 00319007. doi: 10.1103/PhysRevLett.100.014502.

[45] N. Vilanova, V. R. Gundabala, and a. Fernandez-Nieves. Drop size control in electro-coflow. *Applied Physics Letters*, 99(2):2–5, 2011. ISSN 00036951. doi: 10.1063/1.3610949.

[46] J. R. Melcher and G. I. Taylor. Electrohydrodynamics - A review of the role of interfacial shear stresses. ISSN 0066-4189. doi: 10.1146/annurev.fl.01.010169.000551.

[47] Jr Melcher. *Continuum Electromechanics*. ISBN 9780262131650.

[48] Wilko Rohlfs, Georg F. Dietze, Herman D. Haustein, and Reinhold Kneer. Two-phase electrohydrodynamic simulations using a volume-of-fluid approach: A comment. *Journal of Computational Physics*, 231(12):4454–4463, 2012. ISSN 00219991. doi: 10.1016/j.jcp.2012.02.003.

[49] GI Taylor and AD McEwan. The stability of a horizontal fluid interface in a vertical electric field. *Journal of Fluid Mechanics*, 22(01):1–15, 1965.

[50] Ed Wilkes, Sd Phillips, and Oa Basaran. Computational and experimental analysis of dynamics of drop formation. *Physics of Fluids*, (12):3577–3598. ISSN 1070-6631. doi: 10.1063/1.870224.